

## Eocene magmatism related to postcollisional extension in the Eastern Pontides (NE Türkiye): $^{40}\text{Ar}$ - $^{39}\text{Ar}$ geochronology, geochemistry, and whole-rock Sr-Nd-Pb-Hf isotopes

EMRE AYDINÇAKIR

CEM YÜCEL

ABDULLAH KAYGUSUZ

ÖZGÜR BİLİCİ

SİNAN YILMAZER

See next page for additional authors

Follow this and additional works at: <https://journals.tubitak.gov.tr/earth>



Part of the Earth Sciences Commons



This work is licensed under a [Creative Commons Attribution 4.0 International License](https://creativecommons.org/licenses/by/4.0/).

---

**Eocene magmatism related to postcollisional extension in the Eastern Pontides (NE Türkiye):  $^{40}\text{Ar}$ - $^{39}\text{Ar}$  geochronology, geochemistry, and whole-rock Sr-Nd-Pb-Hf isotopes**

**Authors**

EMRE AYDINÇAKIR, CEM YÜCEL, ABDULLAH KAYGUSUZ, ÖZGÜR BİLİCİ, SİNAN YILMAZER, and GILLES RUFFET

## Eocene magmatism related to postcollisional extension in the Eastern Pontides (NE Türkiye): $^{40}\text{Ar}$ - $^{39}\text{Ar}$ geochronology, geochemistry, and whole-rock Sr-Nd-Pb-Hf isotopes

Emre AYDINÇAKIR<sup>1\*</sup>, Cem YÜCEL<sup>2</sup>, Abdullah KAYGUSUZ<sup>1</sup>, Özgür BİLİCİ<sup>3</sup>,  
Sinan YILMAZER<sup>4</sup>, Gilles RUFFET<sup>5,6</sup>

<sup>1</sup>Department of Geological Engineering, Faculty of Engineering and Natural Sciences, Gümüşhane University, Gümüşhane, Türkiye

<sup>2</sup>Department of Mining Engineering, Faculty of Engineering and Natural Sciences, Gümüşhane University, Gümüşhane, Türkiye

<sup>3</sup>Department of Civil Engineering, Faculty of Engineering, Atatürk University, Erzurum, Türkiye

<sup>4</sup>Eurasia Institute of Earth Sciences, İstanbul Technical University, İstanbul, Türkiye

<sup>5</sup>The National Centre for Scientific Research (CNRS)/The National Institute for Earth Sciences and Astronomy (INSU) UMR6118, Geosciences Rennes, University of Rennes 1, Rennes, France

<sup>6</sup>Geosciences Rennes, University of Rennes 1, Rennes, France

Received: 30.10.2023 • Accepted/Published Online: 22.05.2024 • Final Version: 12.07.2024

**Abstract:** The mineral chemistry, whole-rock geochemistry,  $^{40}\text{Ar}/^{39}\text{Ar}$  dating and Sr-Nd-Pb-Hf isotopes of the Eocene Narman (Erzurum) Volcanic rocks in the southeast of the Eastern Pontides Orogenic Belt (EPOB, NE Türkiye) were investigated. The Narman Volcanites consist of basaltic dyke, basaltic lava, and basaltic volcanic breccia facies. Volcanites contain plagioclase ( $\text{An}_{34-80}$ ), clinopyroxene ( $\text{Wo}_{38-47}\text{En}_{41-50}\text{Fs}_{5-18}$ ), and olivine ( $\text{Fo}_{68-90}$ ) as phenocrystals with magnetite/titanomagnetite microphenocrysts. New  $^{40}\text{Ar}$ - $^{39}\text{Ar}$  ages suggest that these volcanic rocks erupted between  $44.5 \pm 0.1$  and  $43.4 \pm 0.1$  Ma, within the Middle Eocene (Lutetian). Narman Volcanites have calc-alkaline character, with medium-high K content. Volcanites are enriched in large ion lithophile elements (LILE) and light rare earth elements (LREE), while they are depleted in terms of high field strength elements (HFSE). Chondrite-normalized rare earth element distributions have concave shape with moderate enrichment ( $\text{La}_N/\text{Lu}_N = 2.78-7.99$ ), leading to consideration that the magmas forming the volcanics derived from similar sources. Isotopically, the rocks in the Narman Volcanites have low-medium initial  $^{87}\text{Sr}/^{86}\text{Sr}$  values (0.70405–0.70485), initial  $^{143}\text{Nd}/^{144}\text{Nd}$  values (0.512606–0.512848) and positive  $\text{Nd}_i$  (+0.5 – +5.2). Depleted mantle Nd model ages were  $T_{\text{DM1}} = 0.29-0.62$  Ga and  $T_{\text{DM2}} = 0.43-0.83$  Ga.  $(^{206}\text{Pb}/^{204}\text{Pb})_i$ ,  $(^{207}\text{Pb}/^{204}\text{Pb})_i$ , and  $(^{208}\text{Pb}/^{204}\text{Pb})_i$  values vary in the ranges of 18.246–18.709, 15.578–15.616, and 38.225–38.791, respectively. The initial  $(^{176}\text{Hf}/^{177}\text{Hf})_i$  ratios for the volcanites are between 0.282770 and 0.283013, while the  $\epsilon\text{Hf}$  values range from +7.6 to +9.

All the evidence supports the conclusion that the parental magma for the rocks probably derived from an enriched lithospheric mantle, previously metasomatized by fluids derived from subducted slab during asthenospheric upwelling, due to fragmented asymmetric delamination in a postcollisional extensional tectonic environment.

**Key words:**  $^{40}\text{Ar}$ - $^{39}\text{Ar}$  thermochronology, mineral chemistry, postcollisional setting, delamination, Eastern Pontides, Türkiye

### 1. Introduction

The Eastern Pontides Orogenic Belt (EPOB) is located east of the Sakarya Zone (northern Türkiye, Figure 1a) and is considered one of the most complicated and important sections of the Alpine-Himalayan system due to sequential subduction and collision events (Şengör and Yılmaz, 1981; Okay and Sahinturk, 1997; Yılmaz et al., 1997). The Eastern Pontides formed when the Neo-Tethys Ocean was subducted under the Eurasian plate to the north and is accepted as being a well-preserved arc system in the Early Jurassic and Late Cretaceous (Figure

1a). From the past to the present, numerous authors have studied the geodynamic evolution of the EPOB (Şengör and Yılmaz, 1981; Okay and Sahinturk, 1997; Yılmaz et al., 1997; Okay and Tüysüz, 1999; Altunkaynak, 2007; Keskin et al., 2008; Dilek et al., 2010; Temizel et al., 2012; Ustaömer et al., 2013; Arslan et al., 2013, 2022; Aydınçakır and Şen, 2013; Aydınçakır et al., 2022; Ersoy et al., 2017; Özdamar et al., 2017; Yücel et al., 2017; Göçmengil et al., 2018; Dokuz et al., 2019; Aydın et al., 2020; Kaygusuz et al., 2022). Understanding the features of Eocene magmatism is very important in terms of interpreting the geodynamic

\* Correspondence: aydinçakir61@gmail.com

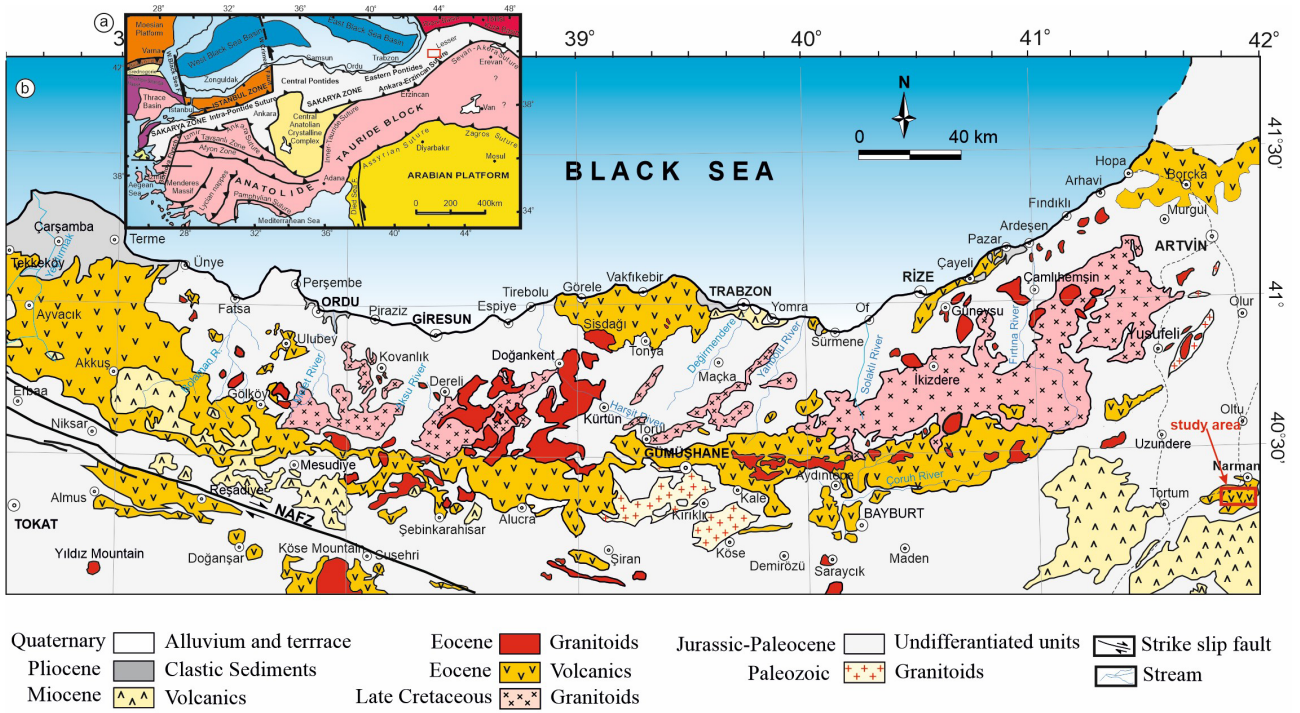


**Figure 1.** (a) The tectonic units and the main suture zones of Türkiye (after Okay and Tüysüz 1999); (b) the simplified geological map of the Eastern Pontides showing distribution of the Eocene and Miocene–Quaternary volcanic rocks. Modified after Güven (1993)<sup>1</sup>, Arslan et al. (2013), Aydınçakır and Şen (2013), Temizel et al. (2016), Yücel (2019), and Kaygusuz et al. (2022).

<sup>1</sup>Güven IH (1993). Doğu Pontidler'in 1:25000 ölçekli jeolojisi ve kompilasyonu [1:25000 scale geology and compilation of the Eastern Pontide] (unpublished). Ankara, Türkiye: General Directorate of Mineral Research and Exploration (MTA).

evolution of the region. There are ongoing debates about whether the Eocene magmatism, which covers a very wide area in the EPOB, is subduction-related or postcollisional, resulting from the collision of the Anatolide-Tauride block with the Pontides during the closure of the northern branch of the Neo-Tethys Ocean (Robertson et al., 2006; Eyuboglu et al., 2011; Temizel et al., 2012; Arslan et al., 2013, 2022; Aydınçakır and Şen, 2013; Aydınçakır et al., 2022; Yücel et al., 2017; Göçmengil et al., 2018; Kaygusuz et al., 2022, 2024). Eocene volcano-sedimentary and intrusive rocks cover a large area of Türkiye (Robertson et al., 2006; Keskin et al., 2008; Aydınçakır and Şen, 2013; Gülmez et al., 2013; Arslan et al., 2013; Yücel et al., 2017; Ersoy et al., 2017; Özdamar et al., 2017; Göçmengil et al., 2018; Aydınçakır et al., 2022; Arslan et al., 2022) and Iran (Stern et al., 2021). Some models related to widespread Eocene magmatism were proposed: (1) collisional slab breakoff under the İzmir–Ankara–Erzincan Suture Zone (İAESZ, Altunkaynak, 2007; Dilek et al., 2010), (2) back-arc expansion events related to northward subduction along the Bitlis Zagros Suture Zone (BZSZ, Robertson et al., 2006), (3) postcollisional crustal thickening and delamination of thickened crust along the IAES (Karsli et al., 2011; Aydınçakır and Şen, 2013; Aydınçakır et al., 2020;

2022), and (4) slab window-related processes (Eyuboglu et al., 2011).

This study provides important clues to understanding petrogenetic processes for Eocene volcanic rocks in the Narman (Erzurum) region at the easternmost point of the EPOB. This article presents new <sup>40</sup>Ar–<sup>39</sup>Ar dating, Sr–Nd–Pb–Hf isotopes, and whole-rock geochemical data for Middle Eocene volcanic rocks at the southeastern end of the Eastern Pontides (Figure 1b). Our objectives are to clarify the petrogenesis and tectonomagmatic evolution of the volcanic rocks in the region and to characterize the geodynamic evolution of the Eastern Pontides during the Eocene.

## 2. Regional and local geology

The Eastern Pontides are a subset of the Sakarya zone, which is one of the major tectonic units in Türkiye (Figure 1a, Okay and Tüysüz, 1999). The Sakarya Zone is a strip-like continent that extends from the Biga Peninsula to the Lesser Caucasus located in the north of Türkiye. This region is surrounded by Rhodope-Istranca to the northwest, İstanbul and Zonguldak regions and the Central and Eastern Pontides. This tectonic unit comprises a chain of mountains that are 200 km width and 500 km length, and

it is accepted as part of the Alpine orogenic system. The basement rocks of the Sakarya Zone comprise pre-Variscan gneiss and schists (Topuz et al., 2004) and metasediments that accumulated in Cadomian sedimentary basins (Dokuz et al., 2022). These units are intruded by Ordovician, Early Cambrian and Silurian-Devonian metagranites (Karsli et al., 2020a), and Middle-Late Carboniferous granitoid (Topuz et al., 2010; Dokuz, 2011; Kaygusuz et al., 2012). This basement is unconformably overlain by Permo-Carboniferous shallow marine-terrestrial sedimentary rocks observed around Pulur (Okay and Leven, 1996). Early-Middle Jurassic volcanoclastic and sedimentary rocks unconformably overlie basement rocks (Şen, 2007; Kandemir and Yılmaz, 2009). The pre-Jurassic basement rocks are cut by Early and Middle Jurassic intrusive rocks (Eyuboglu et al., 2016; Dokuz et al., 2017; Karsli et al., 2017; Saydam Eker and Arı, 2020; Aydınçakır et al., 2020, 2023). The Late Jurassic-Early Cretaceous period passed very calmly in terms of tectonic movements and magmatic activity. In Late Cretaceous time, the Eastern Pontides represented a magmatic arc developing with northward subduction of the Neo-Tethys along the Sakarya Zone (Okay and Sahinturk, 1997; Yılmaz et al., 1997). The subduction direction and geotectonic evolution of the Eastern Pontides in the Cretaceous is controversial. Numerous researchers proposed that the Eastern Pontides are a magmatic arc resulting from northward subduction of the Neo-Tethys along the south margin of the Sakarya Zone (Okay and Sahinturk, 1997; Yılmaz et al., 1997; Kaygusuz and Aydınçakır, 2009; Uysal et al., 2014; Aydınçakır, 2016; Özdamar, 2016; Temizel et al., 2019; Aydin et al., 2020; Kaygusuz et al., 2021; Yücel et al., 2024). Conversely, others proposed southward subduction that continued uninterrupted from the Paleozoic period until the end of the Eocene period (Dewey et al., 1973; Eyuboglu et al., 2011). The Eastern Pontides are dominated by plutonic and volcanic rocks with facies variations in north-south direction (Karsli et al., 2012; Arslan et al., 2013; Yücel et al., 2017; Dokuz et al., 2019; Temizel et al., 2020; Aydınçakır et al., 2022). From the Paleocene to Early Eocene, the Eastern Pontides was above sea level, probably because of the collision between the Pontides magmatic arc and the Tauride-Anatolide Platform (TAP, Okay and Sahinturk 1997; Boztuğ et al., 2004). This caused common compression, crustal elevation and thickening, and flysch accumulation. Adakitic and nonadakitic rocks with Early Eocene age (54–48 My) occurred in the final stage of arc-continent collision (Eyuboglu et al., 2011; Topuz et al., 2011; Karsli et al., 2011; Aydınçakır, 2014; Gücer, 2021). During the Middle Eocene, postcollisional volcano-sedimentary rocks and calc-alkaline shoshonitic plutons developed (Karsli et al., 2012; Arslan et al., 2013; Yücel et al., 2017; Kaygusuz et al., 2018, 2022; Dokuz et al., 2019; Temizel

et al., 2020; Aydınçakır et al., 2022). Miocene-Pliocene-Quaternary volcanic rocks, mostly alkali with lower rates of calc-alkali composition, are the youngest representatives of magmatic activity in the Eastern Pontides (Karsli et al., 2008, 2020b; Kaygusuz, 2009; Eyuboglu et al., 2012; Dokuz et al., 2013; Yücel et al., 2017; Yücel, 2019).

The study area is in the east part of the EPOB (Figures 1b and 2). The basement for units in the study area comprises volcanoclastic rocks representing andesitic, basaltic, trachytic lava, and pyroclastic units, defined as the Karataş Formation (Bozkuş, 1992, as cited in Konak and Hakyemez, 2008). The unit is covered above an angular unconformity by the Narman volcanic rocks comprising olivine basalt and pyroclastic rocks (Konak and Hakyemez, 2001). Due to its location above and below the Narman Volcanics, the Oltu Formation is considered to be the lateral transition of this unit. The Oltu Formation comprises white gypsum and limestone interlayers containing coal seams, and yellow-red-green pebblestone, sandstone and mudstone. The age of the unit was given as Late Oligocene-Early Miocene by Benda (1971). The Early Miocene Alabalık Formation occurs above the Oltu Formation with conformable transition and is represented by yellow-green tuff, agglomerate and epiclastic levels (Figure 2, Bayraktutan, 1994).

### 3. Analytical methods

#### 3.1. Electron microprobe analysis

Based on petrographic observations and photomicrography, the newest and most representative volcanic rock samples from volcanic rocks were chosen to determine the mineral composition. The major element composition of the minerals (feldspar, hornblende, brown mica, clinopyroxene, and Fe-Ti oxides) from carbon-coated polished sections were analyzed using a CAMECA SX100 instrument from the IFREMER EPMA Laboratories (Brest, France) with accelerating voltage of 15 kV and a sample current of 15 nA. The peak and background counting times ranged from 10 to 20 s and from 5 to 10 s, respectively. Natural minerals and synthetic/compounds were used as standards. The matrix effects were corrected by using Phi ( $\rho$ ) z Peak Sight software from CAMECA. Typical standard deviations ( $1\sigma$ ) ranged from 0.1 to 0.3 wt.% for Si, Ca, Na, and Al and from 0.03 to 0.1 wt.% for Fe, Cr, K, Ti, Mg, and Mn.

#### 3.2. Whole-rock major and trace element analysis

Twenty-five samples were selected for major and trace element analysis. To prepare the rock powders, 0.5–1 kg of the fresh samples was crushed in a steel crusher, and then, the samples were ground in an agate mill to obtain grain sizes of <200 mesh. The major and trace element contents were determined at the commercial ACME Laboratories Ltd. in Vancouver, Canada. The major element oxides of

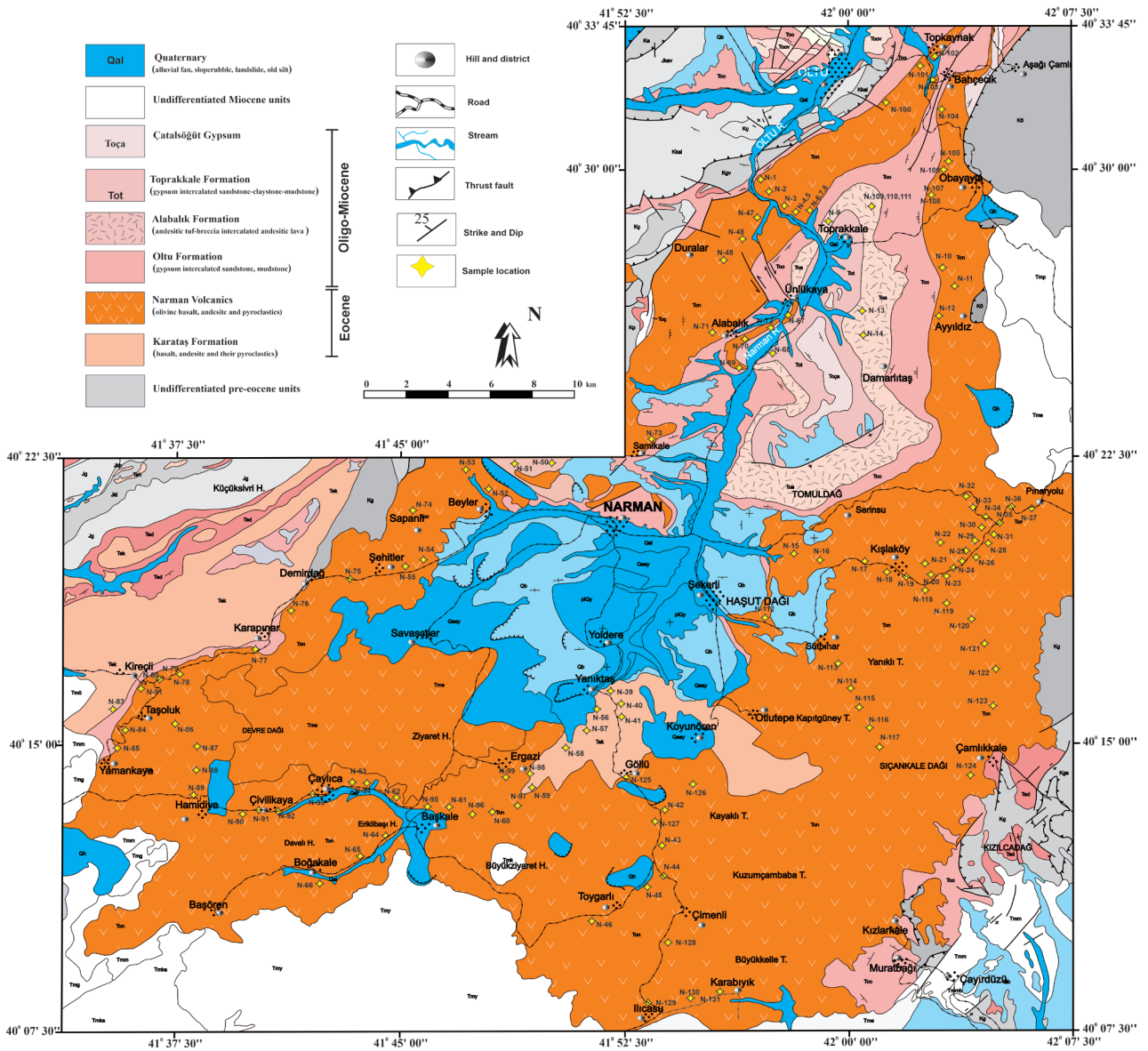


Figure 2. (a) The geological map of the Narman (Erzurum) area, and the sample locations.

the samples were measured by ICP-ES for major oxides (0.2 g pulp sample by  $\text{LiBO}_2$  fusion). The detection limits are approximately 0.001–0.1 wt.%. For the trace elements, 0.2 g of the sample powder and 1.5 g of  $\text{LiBO}_2$  flux were mixed in a graphite crucible and subsequently heated to 1050 °C for 15 min in a muffle furnace. The molten sample was then dissolved in 100 mL of 5%  $\text{HNO}_3$ . Sample solutions were shaken for 2 h, and then, an aliquot was poured into a polypropylene test tube and aspirated into the Perkin-Elmer Elan 600 ICP mass spectrometer. Calibration and verification standards (STD-SO-19), together with reagent blanks, were added to the sample sequence. The detection limits determine the range from 0.01 to 0.5 ppm for most trace elements.

### 3.3. Sr–Nd–Pb–Hf isotope analysis

Sr, Nd, and Pb isotope compositions of selected samples from the plutons were performed at the Department of Geological Sciences, New Mexico State University. All isotopic measurements were conducted using TIMS on a VG Sector 30 mass spectrometer. Samples were loaded onto rhenium filaments either on the cathode bead of a single filament or on the side filament of a triple-filament assembly. The reproducibility of  $^{87}\text{Rb}/^{86}\text{Sr}$  and  $^{147}\text{Sm}/^{144}\text{Nd}$  ratios is within 0.3%, and  $^{87}\text{Sr}/^{86}\text{Sr}$  and  $^{143}\text{Nd}/^{144}\text{Nd}$  ratios are within  $\pm 0.000025$  and  $\pm 0.00003$ , respectively. NBS 987 standard analyses yielded values of 0.710226 (11), 0.710213 (13), 0.710219 (10), and 0.710260 (11). Pb isotopes were analyzed using the middle filament position

of a Cathodeon bead assembly. Samples were loaded using 5% HNO<sub>3</sub> in a matrix composed of silica gel and phosphoric acid. Approximately 2 µL of silica gel was positioned on the filament, and 1 µL of phosphoric acid was added. Standards were also loaded and analyzed using the same procedures. The mean values of the standards were  $^{206}\text{Pb}/^{204}\text{Pb} = 16.844$ ,  $^{207}\text{Pb}/^{204}\text{Pb} = 15.379$ , and  $^{208}\text{Pb}/^{204}\text{Pb} = 36.199$ . Deviations from standards are within 0.2%. Detailed analytical procedures for Sr, Nd, and Pb isotopic measurements are provided by Ramos (1992).

### 3.4. Ar-Ar dating

Three single groundmass fragments from the studied dikes were analyzed by the continuous laser probe (CO<sub>2</sub> Synrad) stepwise heating  $^{39}\text{Ar}$ - $^{40}\text{Ar}$  technique at Geosciences Rennes (France).

The samples were wrapped in Al foil to form small packets (11 × 11 mm) that were stacked up to form columns within which packets of fluence monitors were inserted every 10 samples. Irradiation was performed at the McMaster Nuclear Reactor (Hamilton, Canada) and used 5C high flux location without Cd shielding. It lasted 13.42 h (J/h ≈  $3.71 \times 10^{-4} \text{ h}^{-1}$ ). The irradiation standard was sanidine TCRs ( $28.608 \pm 0.033 \text{ Ma}$ ; according to Renne et al., 1998, 2010, 2011). The sample arrangement in the irradiation allowed us to monitor the flux gradient with a precision of ± 0.2%.

Heating steps were performed with a CO<sub>2</sub> laser probe. All experiments concerned single grains. The experimental procedure was described by Ruffet et al. (1991, 1995). The five argon isotopes and the background baselines were measured in 11 cycles in peak-jumping mode. Blanks were performed routinely every first or third/fourth run and subtracted from subsequent sample gas fractions. All isotopic measurements are corrected for K, Ca, and Cl isotopic interferences, mass discrimination and atmospheric argon contamination.

Apparent age errors are plotted at the 2s level and do not include the errors on the  $^{40}\text{Ar}^*/^{39}\text{Ar}_k$  ratio and age of the monitor and decay constant. The errors on the  $^{40}\text{Ar}^*/^{39}\text{Ar}_k$  ratio and age of the monitor and decay constant are included in the final calculation of the (pseudo-) plateau age error margins or for apparent ages individually cited. The analyses were performed on a Map215 mass spectrometer.

## 4. Results

### 4.1. Field and petrographic content

The unit crops out in the study area, mainly in an area containing Oltu and Narman districts in the north, Ilıcasu in the south, Çamlıkaya in the east and Başören in the west. The studied Eocene volcanic rocks are generally observed as pyroclastics, lava flows, and dikes.

Pyroclastic rocks comprise angular rock fragments with diameters varying from 2 cm to block size (Figures 3a and 3b). The groundmass for breccia fragments within the rock is generally tuff, with the breccia-pebble ratio reaching nearly 70%. Fresh fractured surfaces are dark gray-black color. They contain abundant amounts of mafic mineral phenocrysts.

Basaltic volcanic breccia: These generally have hyalomicroclitic, porphyritic, and glomeroporphyritic texture with modal mineralogy comprising plagioclase, clinopyroxene, olivine phenocrystals, and Fe-Ti oxides.

Basaltic dykes: These were emplaced by cutting basaltic lava and pyroclastics. Most dykes have fresh appearance, while weathered surfaces generally have light brown-beige color, and fresh surfaces have dark gray-black color (Figure 3c). Dykes have massive structures and strikes are generally NE-SW. The width of dykes varies from 30 cm to 2–3 m. Basaltic dyke samples comprise clinopyroxene, olivine, plagioclase, and Fe-Ti oxide minerals. They generally display microclitic, porphyritic, poikilitic, intersertal, and occasionally glomerophyritic textures (Figures 4a and 4b). Clinopyroxene is generally euhedral to anhedral and is observed as mega and phenocrystals and anhedral micrograins in the groundmass. This crystal is corroded by groundmass, has sieve texture, and contains mostly opaque and olivine inclusions with remnant centers (Figure 4a). Olivine is generally euhedral and subhedral. They are partly and fully iddingsitized along fractures and edges (Figure 4b). Olivine sometimes occurs as inclusions within clinopyroxenes or displays cumuloaphyric texture with clinopyroxenes. Plagioclase generally forms euhedral phenocrystals and microcrystals and displays albite twinning. Fe-Ti oxide minerals are generally found as subhedral and anhedral crystals around ferromagnesian minerals, as inclusions within clinopyroxenes, and as micrograins in the groundmass. Secondary minerals generally comprise zeolite minerals developing as cavity fill and chlorites developed from ferromagnesian minerals.

Basaltic lava: Massive basalts are present around Narman and Kışlaköy. In the study area, they represent very steep sections of topography above the sedimentary sequence of the Oltu Formation. Massive basalts have macroscopic porphyritic texture, with large augite and plagioclase phenocrystals easily recognized. There are abundant gas cavities, and these cavities are filled with carbonate and silica. Basalts are generally black-purple in color and form thick lava levels. Basalts contain clinopyroxene, plagioclase, and olivine phenocrystals, as well as Fe-Ti oxide minerals and generally have microclitic porphyritic, hyalomicroclitic porphyritic, sieve texture, and glomerophyritic textures (Figures 4c and 4d). Clinopyroxene minerals are observed as megacrystals and phenocrystals and are found as

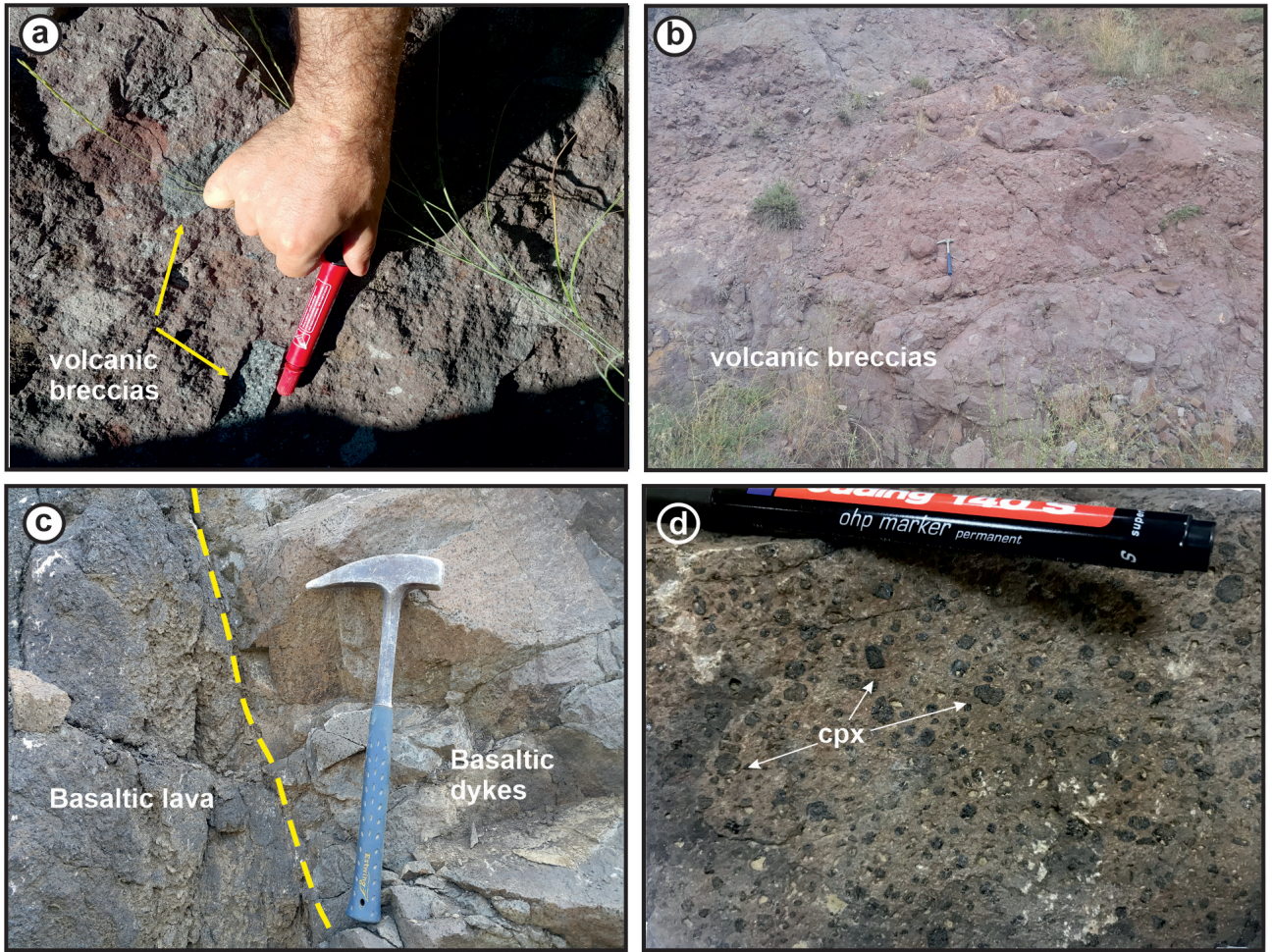


**Figure 3.** General view (a) of the contact between basaltic lava and basaltic dykes, (b) one hand specimen sampled from the basaltic lava with large clinopyroxene phenocryst, (c, d) various-sized breccia fragments constituting pyroclastic rocks and volcanic breccias.

microliths in the groundmass (Figures 4e and 4f). They contain abundant plagioclase, opaque minerals, and olivine inclusions. Zoning is commonly observed in clinopyroxene. Additionally, some clinopyroxenes affected the groundmass and display rough sieve texture (Figures 4e and 4f). Glomerophyritic texture was observed to form where the main clinopyroxene and opaque minerals occur together. Plagioclases are observed as subhedral phenocrystals and as microphenocrystals in groundmass. Generally, they display albite twinning. Sponge-like texture and dissolution by groundmass are very common. Cavities in the sponge-like texture are filled with glass. Some crystals contain both twinning and zoning, while others have a regrowth envelope at the outermost section. Olivine is generally euhedral and found as phenocrystals. Fe-Ti oxide minerals are occasionally found as inclusions and phenocrystals and vary from euhedral to anhedral. They are observed as micrograins in groundmass, and as enclosures within some clinopyroxene and olivine minerals.

#### 4.2. Mineral chemistry

Mineral chemistry analysis for basaltic lava and basaltic dyke samples from the Narman volcanic rocks are presented in Supplementary information. Analyses represent core-mantle-edge compositions for zoned plagioclase and/or at least core and edge analyses for the other minerals. Clinopyroxene in basaltic lava samples consists of diopside and augite with  $Wo_{39-47}En_{41-50}Fs_{5-18}$  composition and  $Mg/(Mg+Fe^{+2})$  ratio of 0.70–0.87 (Figure 5a). Normal and inverse zoning was common in samples. Clinopyroxene in basaltic dyke samples consists of diopside and augite with  $Wo_{38-46}En_{41-50}Fs_{5-18}$  composition and  $Mg/(Mg+Fe^{+2})$  ratio of 0.72–0.89 (Figure 5a). Plagioclase in basaltic lava samples has labradorite ( $An_{51-68}Ab_{29-42}Or_{2-4}$ ) composition, while plagioclase in basaltic dyke samples has labradorite ( $An_{64-69}Ab_{29-33}Or_{2-3}$ ) and bytownite ( $An_{70-80}Ab_{18-28}Or_{1-6}$ ) composition (Figure 5b). Olivine in basaltic lava samples has hyaloserite and chrysolite ( $Fo_{67-90}$ ) composition, while olivine in basaltic dyke samples has hyaloserite



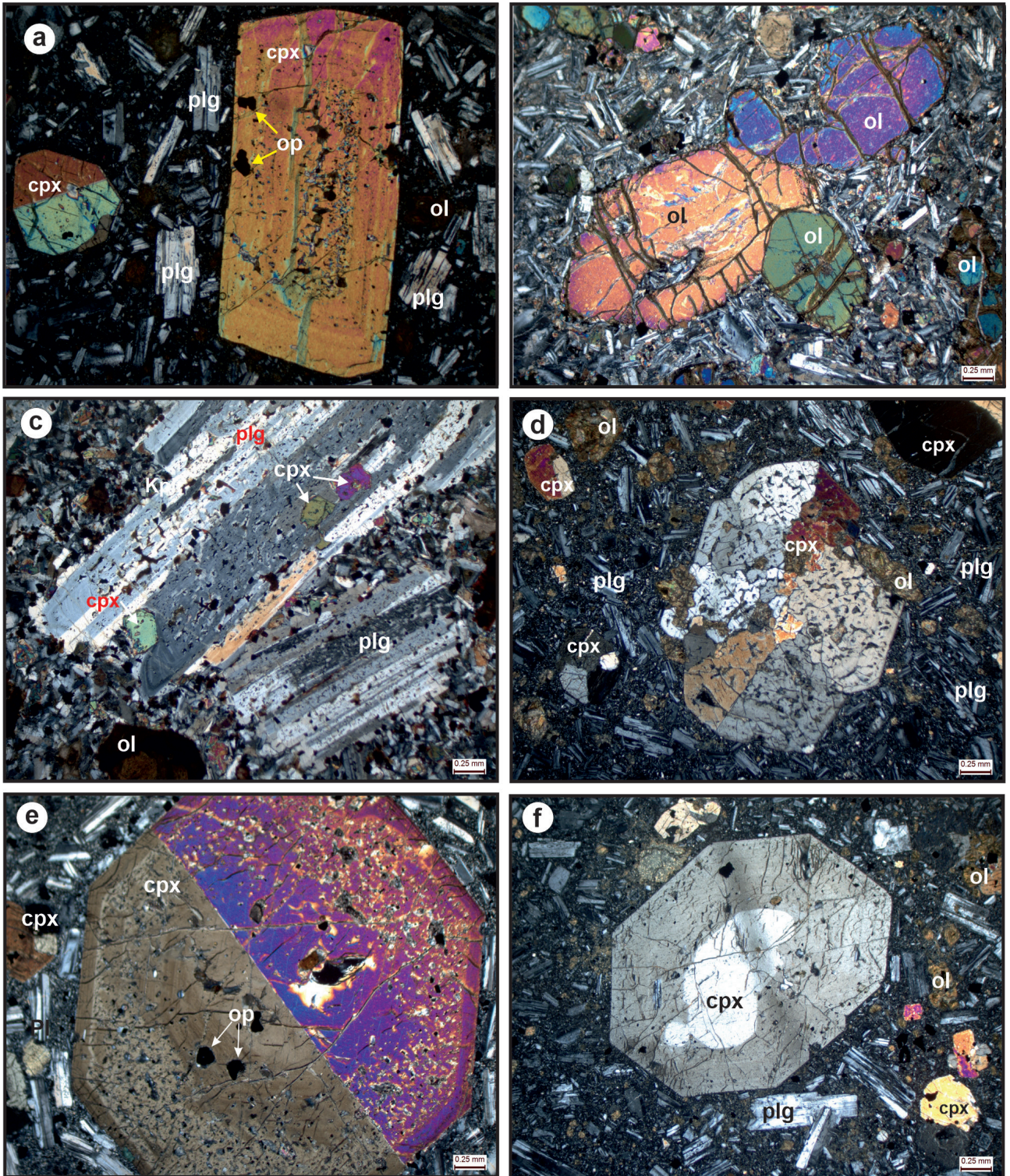


**Figure 4.** Photomicrograph showing textural relationships of the Narman volcanic rocks, (a) clinopyroxene mineral showing zoning and sieve texture in basaltic dykes, (b) euhedral olivine phenocrysts and glomerophytic texture of the basaltic dykes, (c) albite-twinning plagioclase phenocrysts containing clinopyroxene inclusions and sieve texture of the basaltic lava, (d) clinopyroxene phenocryst showing sieve texture in rocks with microlithic-porphyritic texture, (e) euhedral and zoning mega clinopyroxene mineral of basaltic lava, (f) clinopyroxene phenocryst with a sieve texture on the edge and containing a residual center and iddingsitized olivine minerals (plg, plagioclase, cpx, clinopyroxene, ol, olivine, op, opaque mineral).

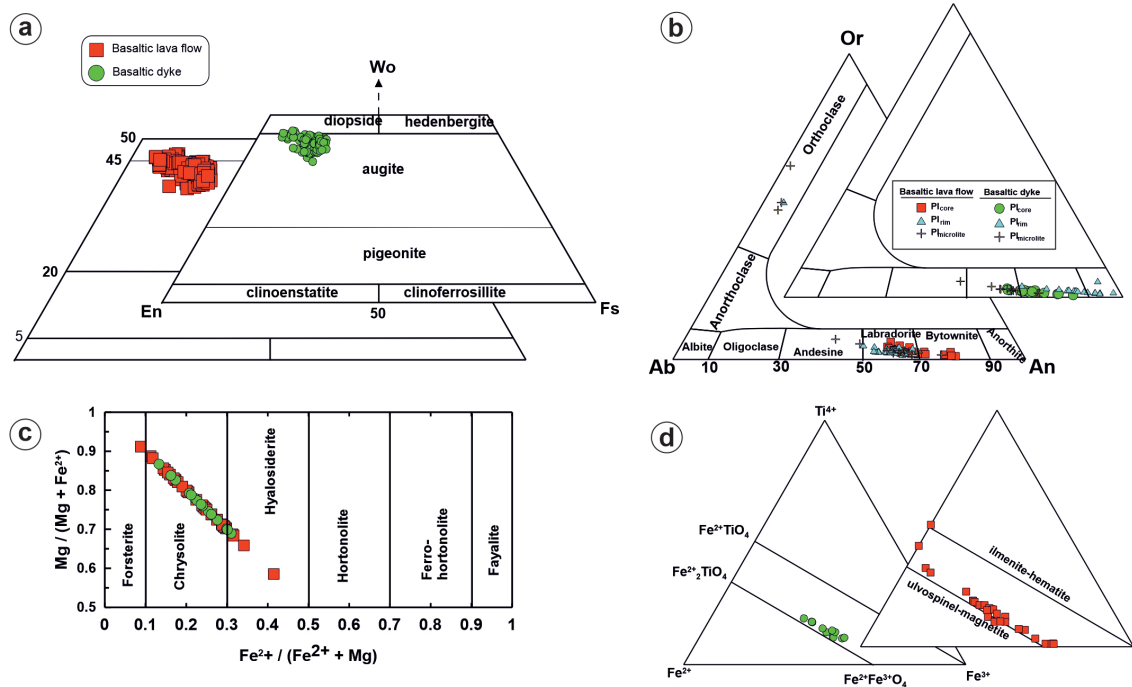


**Figure 5.** (a) Wo-En-Fs ternary plot of pyroxenes (Morimoto et al., 1988), (b) Or-Ab-An ternary plot of plagioclase, (c) olivine classification diagram, and (d)  $Ti^{4+}$ - $Fe^{3+}$ - $Fe^{2+}$  ternary plot of Fe-Ti oxides (Bacon and Hirschmann, 1988) for the volcanic rock samples from the Narman volcanic.

and chrysolite ( $Fo_{68-86}$ ) composition (Figure 5c). Opaque minerals observed as eu-subhedral enclosures within clinopyroxene minerals and within groundmass of basaltic rocks are generally magnetite and titanomagnetite with one ilmenite found. Fe-Ti oxides in basaltic dyke samples had magnetite and titanomagnetite composition (Figure 5d).

#### 4.3. $^{40}Ar$ - $^{39}Ar$ dating

The  $^{40}Ar$ - $^{39}Ar$  age determination for the whole-rock of the three volcanic samples are presented in Supplementary information. A summary of  $^{40}Ar$ - $^{39}Ar$  age determination for volcanic rock samples is also given in Table 1. The step heating experiment results are given as age spectra in Figure 6 and the age spectra and their inverse isochronous calculation results are presented in Supplementary information. The  $^{40}Ar$ - $^{39}Ar$  plateau ages for basaltic lavas within the Narman Volcanites varied from  $43.4 \pm 0.1$  My (N-53) to  $44.5 \pm 0.1$  My (N-33), while  $43.6 \pm 0.1$  My (N-38) was determined to be the age of the basaltic dyke. The ages from  $43.4 \pm 0.1$  to  $44.5 \pm 0.1$  My obtained with  $^{40}Ar$ - $^{39}Ar$  dating indicate the Narman volcanic rocks are Middle Eocene (Lutetian).

#### 4.4. Whole-rock geochemistry

Whole-rock major and trace element analyses for the Narman Volcanics are given in Table 2. According to the  $SiO_2$  versus  $Na_2O+K_2O$  (TAS) diagram by Le Maitre

et al. (1989), basaltic dyke samples plotted in the basalt field, with one sample in the trachybasalt field; basaltic lava samples plotted in the basalt field; and basaltic volcanic breccia plotted in the basaltic andesite field (Figure 7a). Additionally, according to the alkali-subalkali differentiations of Irvine and Baragar (1971), on this diagram, nearly all the samples had subalkali affinity. The  $SiO_2$  composition of Narman volcanic rock samples varies from 46 to 56 wt.%, with Mg numbers from 43 to 71. On the Nb/Y versus  $Zr/TiO_2 \cdot 0.0001$  diagram by Winchester and Floyd (1976), samples from the basaltic dyke fall within the andesite/basalt field, while samples from basaltic lava also fall within the andesite/basalt field. Two samples fall within the alkali-basalt and trachyandesite areas, and samples of basaltic volcanic breccia plot in the andesite field (Figure 7b). Nearly all samples plot in the calc-alkali field on the Th versus Co diagram with basaltic dyke and basaltic lava samples in the basalt field and basaltic volcanic breccia samples in the basaltic andesite field (Figure 7c). On the  $K_2O$  versus  $SiO_2$  diagram (Ewart, 1982), basaltic dyke and basaltic lava samples plot in the medium-high K calc-alkali series, while basaltic volcanic breccia samples plot in the low-medium K calc-alkali series (Figure 7d).

The samples of the basaltic dyke and basaltic lava contain variation of 46–51%  $SiO_2$  content (Table 2). The trends on the  $SiO_2$  versus major oxide and trace element

**Table 1.** A summary of  $^{40}\text{Ar}$ - $^{39}\text{Ar}$  dating results for the Narman volcanic rocks.

Sample no	Material	Lithology	Rock name	Plateau age (Ma)
N-38	Whole-rock	Basaltic dyke	Basalt	$43.6 \pm 0.1$
N-33	Whole-rock	Basaltic lava flow	Basalt	$44.5 \pm 0.1$
N-53	Whole-rock	Basaltic lava flow	Basalt	$43.4 \pm 0.1$

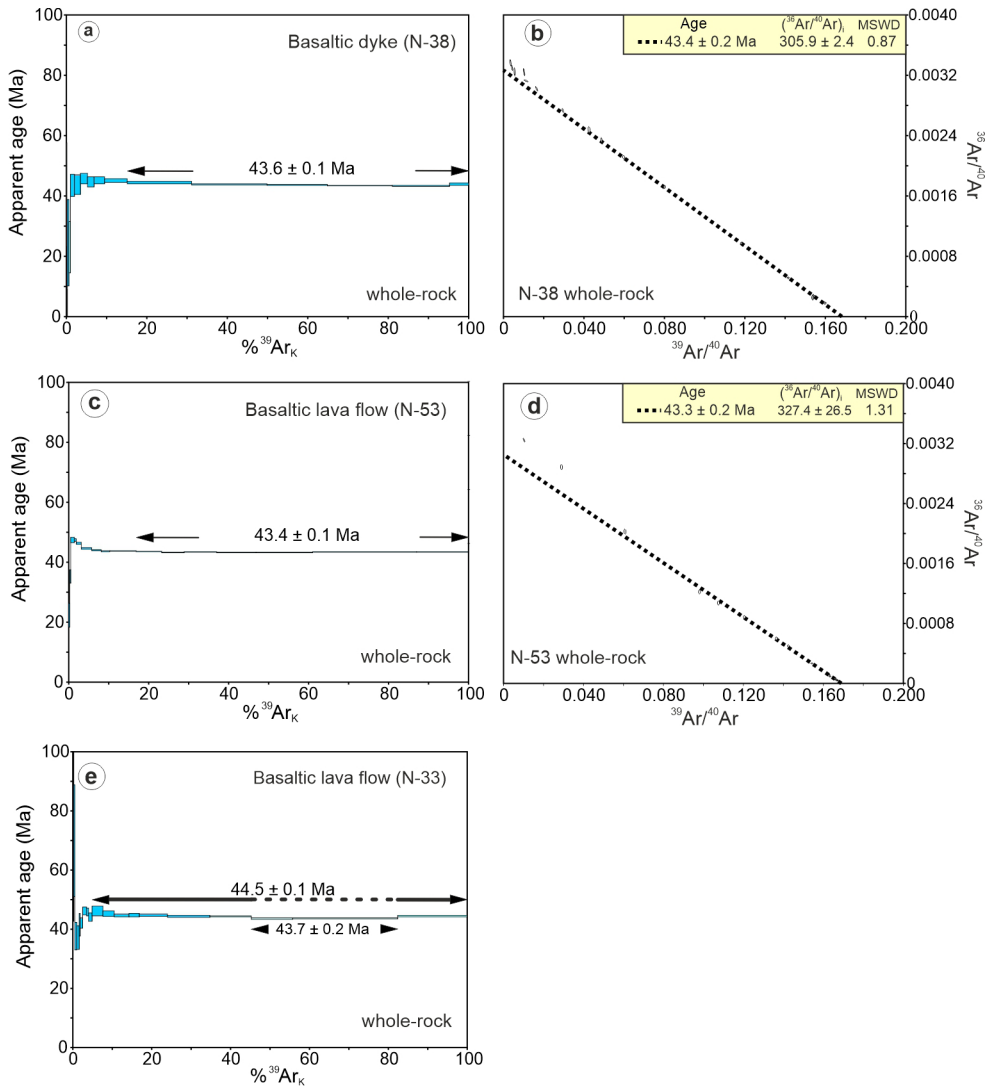


**Figure 6.** (a)  $^{40}\text{Ar}$ - $^{39}\text{Ar}$  ages of the Narman volcanics, (a-b) basaltic dyke (N-38), (c-d-e) basaltic lava flow (N-53, N-33).

variation diagrams (Figure 8) are very clear, with  $\text{Fe}_2\text{O}_3^*$ , CaO, MnO, MgO, Sr, Co, and Ni displaying negative correlations and reducing with increasing  $\text{SiO}_2$ , while  $\text{K}_2\text{O}$ ,  $\text{Na}_2\text{O}$ ,  $\text{P}_2\text{O}_5$ ,  $\text{TiO}_2$ ,  $\text{Al}_2\text{O}_3$ , Ba, Hf, Zr, Rb, Th, Nb, and Y have positive correlations and increase with increasing  $\text{SiO}_2$ . The clear negative trends in the variations of MgO,  $\text{Fe}_2\text{O}_3^*$ , Co, and Ni show that olivine fractionation may have been effective in these rocks. The negative trends on CaO and MgO diagrams indicate clinopyroxene fractionation, while

negative  $\text{Fe}_2\text{O}_3^*$  and MnO trends indicate fractionation of Fe-Ti oxides (Figure 8). The  $\text{SiO}_2$  content of rocks forming basaltic volcanic breccia varies from 53% to 56%. Trends on  $\text{SiO}_2$  versus major oxide and trace element variation diagrams are very clear. With increasing  $\text{SiO}_2$ , CaO, MgO,  $\text{K}_2\text{O}$ ,  $\text{Al}_2\text{O}_3$ ,  $\text{P}_2\text{O}_5$ , MnO and Rb have negative correlations and reduce, while  $\text{Fe}_2\text{O}_3^*$ ,  $\text{Na}_2\text{O}$ ,  $\text{TiO}_2$ , Ba, Hf, Zr, Th, Sr, Nb, Y, and Ni have positive correlations and increase (Figure 8).

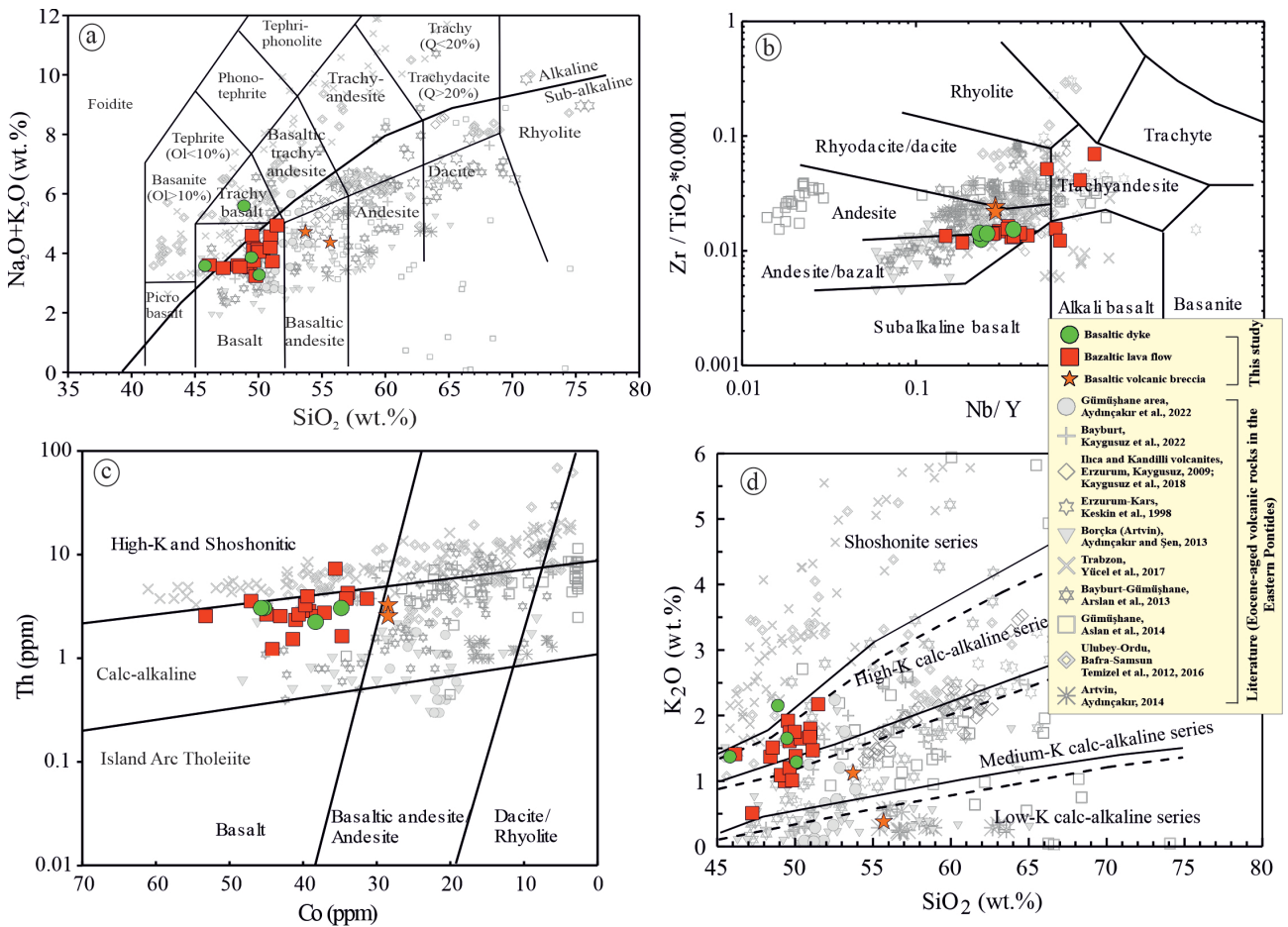


**Figure 7.** Chemical classification and nomenclature plots for the studied volcanic rocks, using (a) the total alkalis versus silica (TAS) diagram (after Le Maitre et al., 1989) (the alkaline and subalkaline discrimination line after Irvine and Baragar, 1971), (b) Zr/TiO<sub>2</sub>\*0.0001 versus Nb/Y diagram (after Winchester and Floyd, 1976), (c) Th versus Co diagram (after Hastie et al., 2007), (d) SiO<sub>2</sub> versus K<sub>2</sub>O plot (after Ewart, 1982). Other data sources for comparison are Middle Eocene volcanic rocks (Keskin et al., 1998; Kaygusuz, 2009; Kaygusuz et al., 2018, 2022; Arslan et al., 2014; Arslan et al., 2013; Aydınçakır and Şen, 2013; Aydınçakır et al., 2022; Aydınçakır, 2014; Temizel et al., 2012, 2016; Yücel et al., 2017).

When trace element diagrams normalized to primitive mantle (Sun and McDonough, 1989) are examined, the studied volcanic rocks generally show pattern of enriched in large ion lithophile elements (LILE: Sr, K<sub>2</sub>O, Rb and Ba), Th and Ce and depleted in high field strength elements (HFSE; Zr, TiO<sub>2</sub> and Y), Nb and Ta content (Figures 9a and 9d). These features in the trace elements in the studied rocks have similar patterns to other Eocene aged volcanic rocks in the region (Figure 9d).

The LILE and HFSE enrichment observed in the Narman volcanic rocks and clear Nb-Ta depletion indicates that these rocks derived from an enriched source rather than a depleted source (Condie et al., 2002). The reason for clear Nb-Ta reduction in melts derived from mantle compared to the primitive mantle (PM) is generally explained by crustal contamination during magma rise and metasomatism associated with subduction (Pearce et al., 1990).

The rare earth element (REE) distributions normalized to chondrite (Taylor and McLennan, 1985) for the studied volcanic rocks are generally similar (Figures 9e and 9h). This situation confirms that the rock assemblage forming the Narman Volcanics derived from the same source. Basaltic lava especially and basaltic volcanic breccia samples display moderate degree of enrichment, while basaltic dyke samples have more enriched distribution compared to the others. Samples from basaltic dykes had (La/Lu)<sub>N</sub> ratio of 5.06–6.47, basaltic lava samples had (La/Lu)<sub>N</sub> ratio of 2.78–7.99, and basaltic volcanic breccia had (La/Lu)<sub>N</sub> ratio of 4.26–5.98. The enrichment in light REE in basaltic lava samples compared to basaltic dyke and basaltic volcanic breccia samples indicates the source of the magma forming basaltic lava was more enriched compared to the source of magma forming the other rocks (Table 2, Figures 9e and 9h). Compared with other



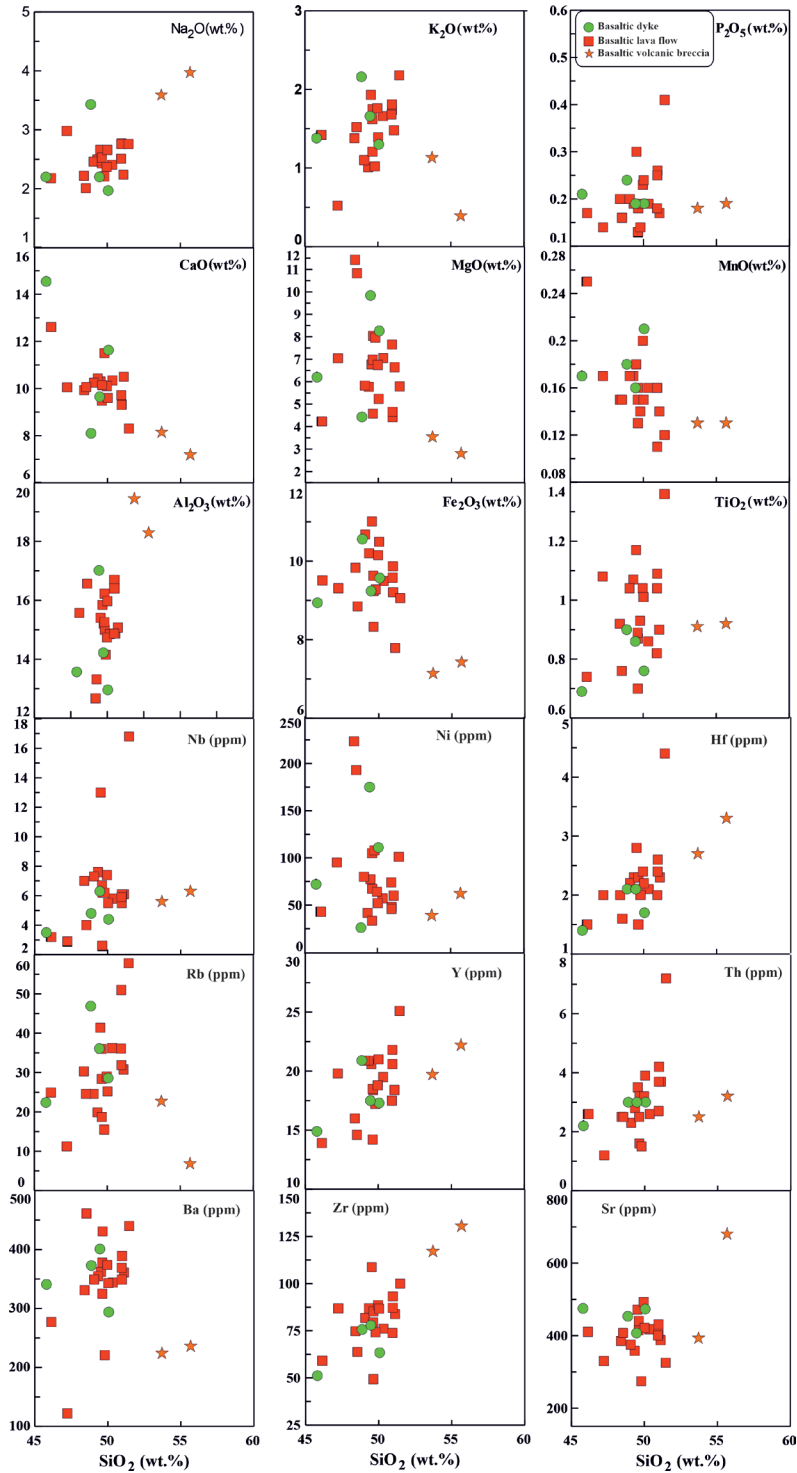
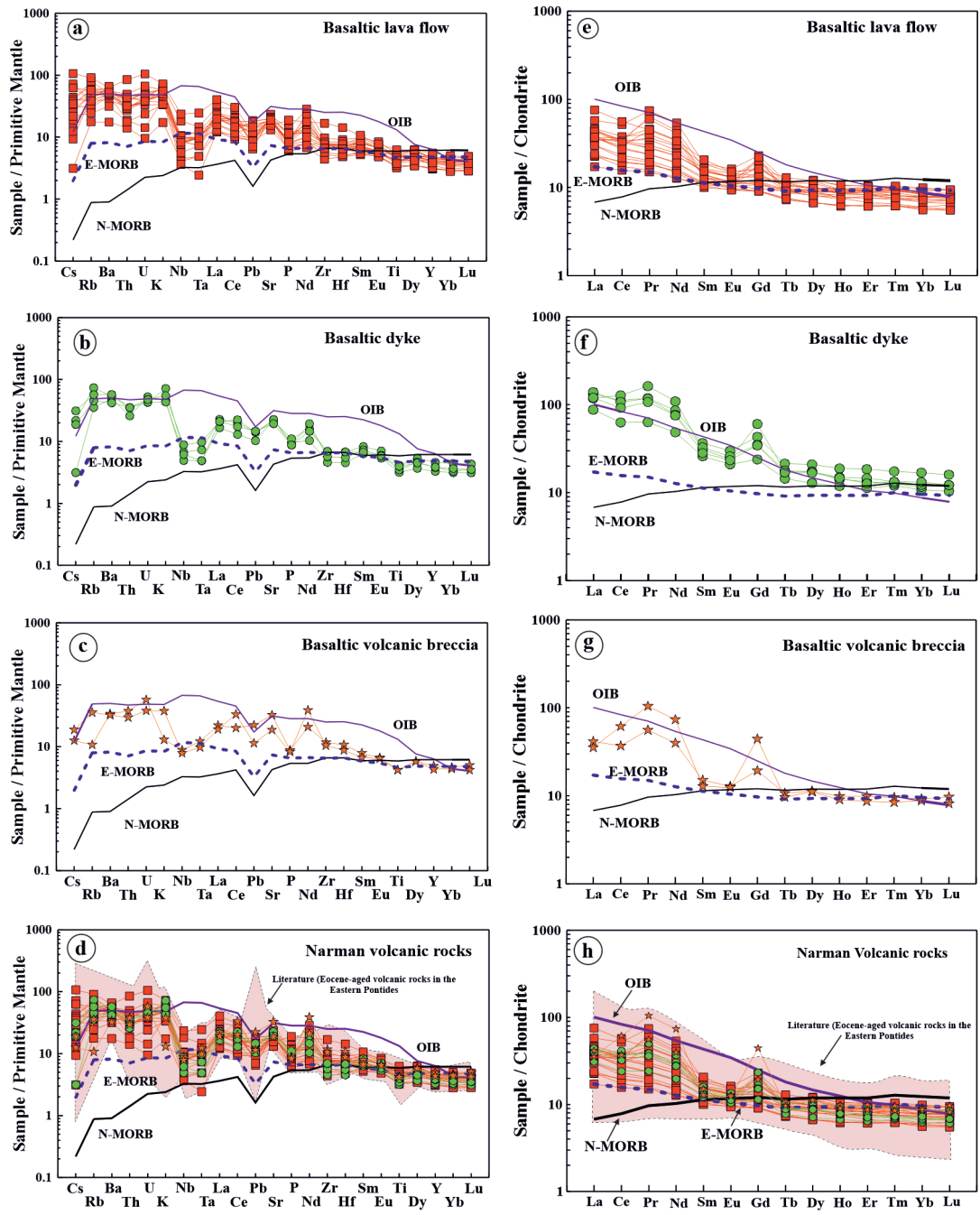


Figure 8. SiO<sub>2</sub>(wt.%) versus major oxide (wt.%), trace element (ppm) variation plots of the Narman volcanic rocks.

Eocene volcanic rocks from the EPOB (e.g., Keskin et al., 1998; Kaygusuz, 2009; Temizel et al., 2012, 2016; Arslan et al., 2013; Aydınçakır and Şen, 2013; Aydınçakır et al., 2022; Aslan et al., 2014; Aydınçakır, 2014; Yücel

et al., 2017; Kaygusuz et al., 2018; 2022), the general geochemical features of the studied volcanic rocks are similar to those of the Eocene volcanic rocks from the EPOB (Figure 9h).



**Figure 9.** (a-d) Primitive mantle-normalized (Sun and McDonough, 1989) spider plots and (e-h) chondrite-normalized (Taylor and McLennan, 1985) rare earth element plots of the Narman volcanic rocks, OIB, N-MORB and E-MORB compositions from Sun and McDonough (1989). Data sources for comparison of other Eocene volcanic rocks are as in Figure 7d.

The REE distributions normalized to chondrite for the volcanic rocks indicated the magmas forming the rocks did not have a significant Eu anomaly, suggesting that plagioclase fractionation did not have much effect in these rocks, or there was high oxygen fugacity (Gill, 1981). The  $(Eu/Eu^*)_N$  ratio varied from 0.62 to 0.88 for

basaltic dykes, 0.63 to 1.04 for basaltic lavas, and 0.44 to 1.00 for basaltic volcanic breccia. Generally, the chondrite-normalized REE distributions for the rocks showed more enrichment in LREE compared to MREE and HREE. The REE distribution diagrams had a concave shape, indicating that clinopyroxene fractionation was effective during the

evolution of volcanic rocks (Thirlwall et al., 1994). All volcanic rocks had  $(Yb)_N < 10$ . This value indicates that garnet was a remnant phase in the mantle source.

#### 4.5. Sr-Nd-Pb-Hf isotope geochemistry

The basaltic lava samples from the Narman Volcanics had initial  $^{87}Sr/^{86}Sr_{(i)}$  ratios from 0.70404 to 0.70445,  $^{143}Nd/^{144}Nd_{(i)}$  ratios varied from 0.512636 to 0.512847, and  $\epsilon Nd_{(45)}$  values were between 1.1 and 5.2 (Table 3). The model age ( $T_{DM}$ ) values calculated for the basaltic lavas varied from 410 to 510 Ma (Table 3). For basaltic dyke samples, initial  $^{87}Sr/^{86}Sr_{(i)}$  ratios were from 0.70476 to 0.70485,  $^{143}Nd/^{144}Nd_{(i)}$  ratios varied from 0.512606 to 0.512706, and  $\epsilon Nd_{(45)}$  values were between 0.5 and 2.43 (Table 3). The  $T_{DM}$  values calculated for the basaltic dyke samples varied from 450 to 620 Ma (Table 3). On the initial Sr and Nd comparison diagrams, they were located in the mantle interval between depleted mantle (DM) and enriched mantle (EMI, EMII) regions (Figure 10a). The  $(^{87}Sr/^{86}Sr)_i$  ratios varying in a narrow interval and the  $\epsilon Nd_i$  values indicate a depleted mantle source region enriched by subducting plate components. On the Sr-Nd diagram (Figure 10a), rocks forming the Narman Volcanics appear to plot between the Eastern Pontide calc-alkali volcanic rocks and the Central Anatolia calc-alkali volcanic rocks on a regional scale.

The basaltic lavas samples of the studied volcanic rocks had  $^{206}Pb/^{204}Pb$  isotope ratios from 18.845 to 18.918,  $^{207}Pb/^{204}Pb$  isotope ratios from 15.607 to 15.621, and  $^{208}Pb/^{204}Pb$  isotope ratios from 38.870 to 38.900 (Table 4). The basaltic dyke samples had  $^{206}Pb/^{204}Pb$  isotope ratios varying from 18.830 to 18.838,  $^{207}Pb/^{204}Pb$  isotope ratios from 15.617 to 15.624, and  $^{208}Pb/^{204}Pb$  isotope ratios from 38.852 to 38.955. On  $^{206}Pb/^{204}Pb$  versus  $^{207}Pb/^{204}Pb$  and  $^{208}Pb/^{204}Pb$  isotope diagrams for the Eocene volcanic rocks, a positive correlation is clearly observed (Figures 10b and 10c). The samples from the investigated rocks are very clearly located in the upper section of the Northern Hemisphere Reference Line (NHRL) (Figures 10b and 10c). Additionally, samples plot between the Enriched Mantle I (EMI) and Enriched Mantle II (EMII) reservoir fields and are closer to the EMII reservoir field. As the EMII reservoir has typical composition for the upper continental crust, while EMI has typical composition for the lower continental crust, enrichment of these mantle reservoirs may be explained by a cycle of upper and lower crustal material mixing in the mantle in subduction zones.

The basaltic lava of the Eocene Narman Volcanics had  $^{176}Lu/^{177}Hf$  ratios ranging from 0.0119 to 0.3332, initial  $^{176}Hf/^{177}Hf$  ratios from 0.282770 to 0.282998, and  $\epsilon_{Hf}$  values varying from +7.6 to +9.2. The rocks forming the basaltic dykes had  $^{176}Lu/^{177}Hf$  ratios of 0.0217 to 0.0176, initial  $^{176}Hf/^{177}Hf$  ratios between 0.282991 and 0.283013, and  $\epsilon_{Hf}$  values varying from +7.9 to +8.6 (Table 5). The Hf isotope

values for the Narman Volcanics are similar to those of mid-oceanic ridge basalts (MORB) and oceanic island basalts (OIB), similar to the Sr-Nd isotope ratios (Figure 10d).

## 5. Discussion

### 5.1. Age

Considering reliable geochronological data, the ages of Eocene volcanic rocks within the Eastern Pontides vary from 37 Ma to 46 Ma (Arslan et al., 2013; Aydınçakır and Şen, 2013; Aslan et al., 2014; Yücel et al., 2017; Aydınçakır et al., 2022; Kaygusuz et al., 2022). In previous studies, the age relations of volcanic rocks were based on volcano-stratigraphic criteria, contact relationships and geochronological studies (Konak and Hakyemez, 2001). The Narman Volcanics were given a Late Oligocene-Early Miocene (?) age based on their position above the Oligocene-Early Miocene Sütkans coals and lateral transition from the Oltu Formation with the same age. Keskin et al. (1998) proposed an age of  $38.5 \pm 0.7$  Ma based on K-Ar dating of one sample from within the volcano-sedimentary unit. In this study, new  $^{40}Ar-^{39}Ar$  dating of Narman volcanic rocks found that the age ranges from  $43.4 \pm 0.1$  Ma to  $44.5 \pm 0.1$  Ma (Lutetian).

### 5.2. Fractional crystallization (FC) and assimilation-fractional crystallization (AFC)

Major and trace element variation diagrams show that fractionation was effective in formation of the volcanic rocks (Figure 8). The reduction in  $TiO_2$  and  $Fe_2O_3^*$  contents with increasing  $SiO_2$  content in the Narman Volcanics shows Fe-Ti oxide fractionation, while negative relationships between  $SiO_2$  versus CaO,  $Fe_2O_3^*$  and MgO indicate fractionation of clinopyroxene phases from the main magma. Chondrite-normalized REE distributions for the volcanic rocks show no clear negative anomaly for Eu values, indicating that plagioclase fractionation was not very effective during the evolution of the rocks (Figures 9e and 9h). Major and trace element distribution diagrams show that clinopyroxene, olivine, plagioclase, Fe-Ti oxide, and apatite fractionation played important roles in the evolution of the studied rocks.

Binary diagrams were prepared using pairs of compatible-incompatible elements to determine the mineral phases affecting fractional crystallization (Figure 11). On these diagrams, the negative trend for increasing Zr versus  $TiO_2$  content indicates Fe-Ti oxide fractionation, while a positive trend indicates clinopyroxene, olivine, plagioclase and apatite fractionation (Figure 11a). The increasing Zr versus positive Y and Nb variations show olivine, clinopyroxene, Fe-Ti oxide, plagioclase and apatite fractionation (Figures 11b and 11c). The negative correlation for Zr versus Ni indicates olivine fractionation (Figure 11d). The positive Sr variation versus Zr represents



**Table 3.** Sr and Nd isotope compositions of samples from the Narman Volcanics.

Sample	Rb (ppm)	Sr (ppm)	<sup>87</sup> Rb/ <sup>86</sup> Sr	<sup>87</sup> Sr/ <sup>86</sup> Sr	2sm	( <sup>87</sup> Sr/ <sup>86</sup> Sr) <sub>i</sub>	Sm (ppm)	Nd (ppm)	<sup>147</sup> Sm/ <sup>144</sup> Nd	<sup>143</sup> Nd/ <sup>144</sup> Nd	( <sup>143</sup> Nd/ <sup>144</sup> Nd) <sub>i</sub>	2sm	e <sub>Nd</sub> (t)	T <sub>Dm</sub> (Ga)
<u>Basaltic dyke (44 Ma)</u>														
N-8	0.06	473.2	0.1748	0.704874	10	0.70476	3.23	26.1	0.0751	0.512728	0.512706	3	2.4	0.4
N-38	0.09	407.1	0.2565	0.705012	10	0.70485	3.00	19.7	0.0925	0.512633	0.512606	4	0.5	0.6
<u>Basaltic lava (45 Ma)</u>														
N36	0.21	503	0.6002	0.704425	10	0.70404	4.62	28.2	0.0367	0.512801	0.512772	3	3.7	0.4
N20	0.09	472	0.2538	0.704615	10	0.70445	4.34	38.3	0.0688	0.512656	0.512636	3	1.1	0.5
N33	0.08	386	0.2273	0.704501	11	0.70436	2.99	29.2	0.0622	0.512779	0.512761	3	3.5	0.4
N53	0.06	493	0.1701	0.704533	10	0.70442	4.24	21.7	0.1187	0.512882	0.512847	3	5.2	0.4

Note: e<sub>Nd</sub> = ((<sup>143</sup>Nd/<sup>144</sup>Nd)<sub>i</sub> / (<sup>143</sup>Nd/<sup>144</sup>Nd)<sub>CHUR</sub> - 1) x 10000, (<sup>143</sup>Nd/<sup>144</sup>Nd)<sub>CHUR</sub> = 0.512638, and (<sup>147</sup>Sm/<sup>144</sup>Sm)<sub>CHUR</sub> = 0.1967 (Jacobsen and Wasserburg, 1980).

Nd model ages (T<sub>Dm</sub>) are calculated with a depleted-mantle reservoir and present-day values of <sup>143</sup>Nd/<sup>144</sup>Nd = 0.513151 and <sup>147</sup>Sm/<sup>144</sup>Sm = 0.219 (Liew and Hofmann, 1988). The model ages were calculated using a linear isotopic ratio growth equation: TDM = 1/x ln(1 + ((<sup>143</sup>Nd/<sup>144</sup>Nd)<sub>i</sub> - 0.513151) / ((<sup>147</sup>Sm/<sup>144</sup>Nd)<sub>i</sub> - 0.2137)).

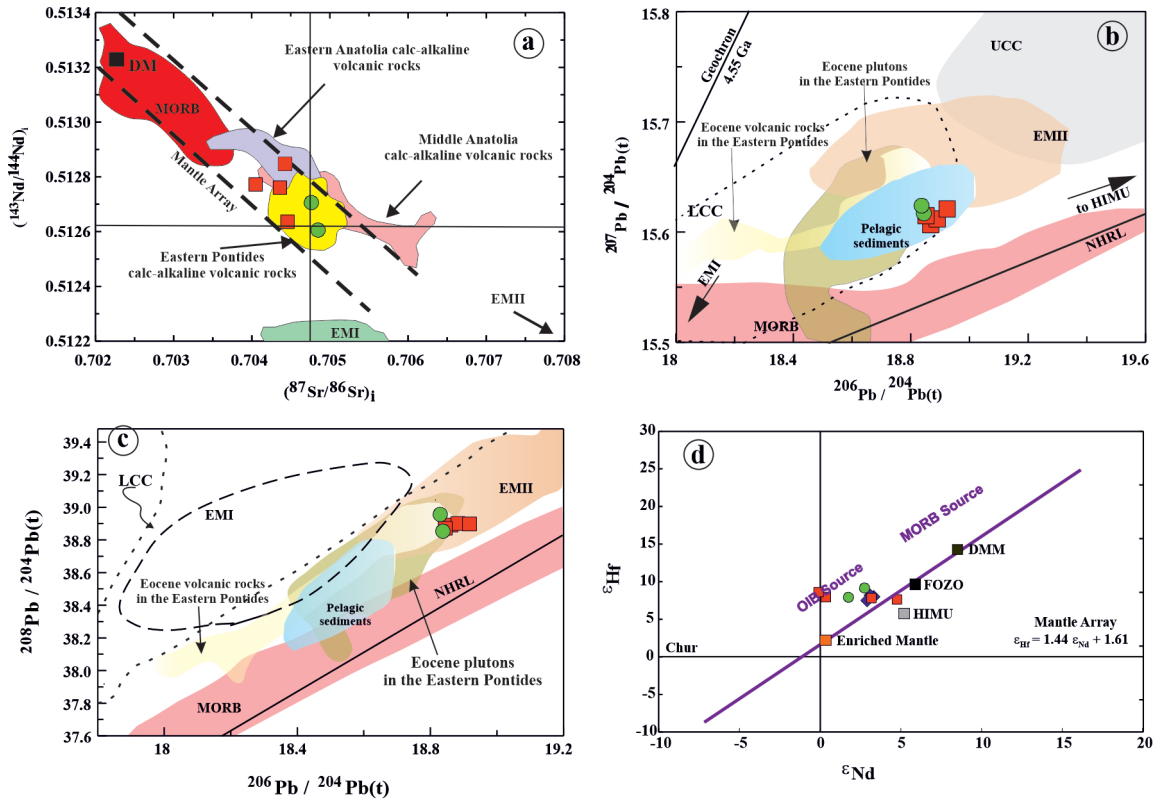


**Figure 10.** (a)  $(^{143}\text{Nd}/^{144}\text{Nd})_i$  versus  $(^{87}\text{Sr}/^{86}\text{Sr})_i$  plot to show the Narman Volcanics. Data for lithospheric mantle array from Davies and von Blanckenburg (1995). Compositions of MORB (mid-ocean ridge basalt) and mantle array from Wilson (1989), Gill (1981) and McCulloch et al. (1994); EMI (enriched mantle type I) and EMII (enriched mantle type II), HIMU (high  $\mu$ : mantle with high U/Th ratio), DM (Depleted Mantle) fields and CHUR (Chondritic Uniform Reservoir)-Sr and -Nd reference lines after Zindler and Hart (1986), Eastern Anatolia calc-alkaline volcanic rocks (Pearce et al., 1990; Buket and Temel, 1998; Keskin et al., 2006), Middle Anatolia calc-alkaline volcanic rocks (Temel et al., 1998; Varol et al., 2007), Eastern Pontides calc-alkaline volcanic rocks (Arslan et al., 2013; Aydınçakır and Şen, 2013; Yücel et al., 2017; Dokuz et al., 2019; Göçmengil et al., 2019; Aydınçakır et al., 2022; Kaygusuz et al., 2022), (b, c)  $^{207}\text{Pb}/^{204}\text{Pb}$  versus  $^{206}\text{Pb}/^{204}\text{Pb}$  and  $^{208}\text{Pb}/^{204}\text{Pb}$  diagrams for the samples of the Narman Volcanics. the composition of the mantle components EM-1 and EM-2 are from (Zindler and Hart, 1986), whereas the composition of subducted sediments is from (Plank and Langmuir, 1998), MORB and crust data are from (Chauvel and Blichert-Toft, 2001). NHRL is after (Vervoort and Blichert-Torft, 1999). Literature data of the Eocene volcanic and plutonic rocks in the Eastern Pontides (Aydınçakır and Şen, 2013; Aydınçakır, 2014; Arslan et al., 2013; Yücel et al., 2017; Aydınçakır et al., 2022; Kaygusuz et al., 2020, 2022), (d)  $\epsilon_{\text{Nd}}$  versus  $\epsilon_{\text{Hf}}$  diagram (the data of EM, DM and  $\mu$  (HIMU) from the study of Stracke (2012); terrestrial range, Vervoort et al. (2011) (symbols are as in Figure 4). Data sources for comparison of other Eocene volcanic rocks are as in Figure 7d.

**Table 4.** Pb isotope compositions of samples from the Narman Volcanics.

Sample	Pb (ppm)	U (ppm)	Th (ppm)	$^{206}\text{Pb}/^{204}\text{Pb}$	$(^{206}\text{Pb}/^{204}\text{Pb})_i$	$^{207}\text{Pb}/^{204}\text{Pb}$	$(^{207}\text{Pb}/^{204}\text{Pb})_i$	$^{208}\text{Pb}/^{204}\text{Pb}$	$(^{208}\text{Pb}/^{204}\text{Pb})_i$
<b>Basaltic dyke (44 Ma)</b>									
N-8	2.60	0.90	3.00	18.838	18.686	15.617	15.610	38.852	38.685
N-38	2.70	1.00	3.00	18.830	18.667	15.624	15.616	38.955	38.794
<b>Basaltic lava (45 Ma)</b>									
N36	2.00	2.80	9.20	18.862	18.232	15.607	15.577	38.890	38.210
N20	1.20	0.90	3.50	18.883	18.546	15.612	15.596	38.900	38.468
N33	1.90	0.90	2.50	18.918	18.705	15.621	15.611	38.896	38.701
N53	1.50	1.10	3.20	18.845	18.515	15.615	15.600	38.870	38.555

**Table 5.** Hf isotope compositions of samples from the Narman Volcanics.

Sample	Lu (ppm)	Hf (ppm)	$^{176}\text{Hf}/^{177}\text{Hf}$	$^{176}\text{Lu}/^{177}\text{Hf}$	$(^{176}\text{Hf}/^{177}\text{Hf})_i$	$\epsilon_{\text{Hf}}$
<u>Basaltic dyke (44 Ma)</u>						
N-8	0.26	1.70	0.283009	0.021692	0.282991	7.9
N-38	0.26	2.10	0.283028	0.017560	0.283013	8.6
<u>Basaltic lava (45 Ma)</u>						
N36	0.37	4.40	0.283006	0.011927	0.282996	7.8
N20	0.28	2.80	0.283010	0.014183	0.282998	8.0
N33	4.70	2.00	0.283044	0.333163	0.282770	9.2
N53	4.04	2.40	0.283001	0.238968	0.282805	7.6

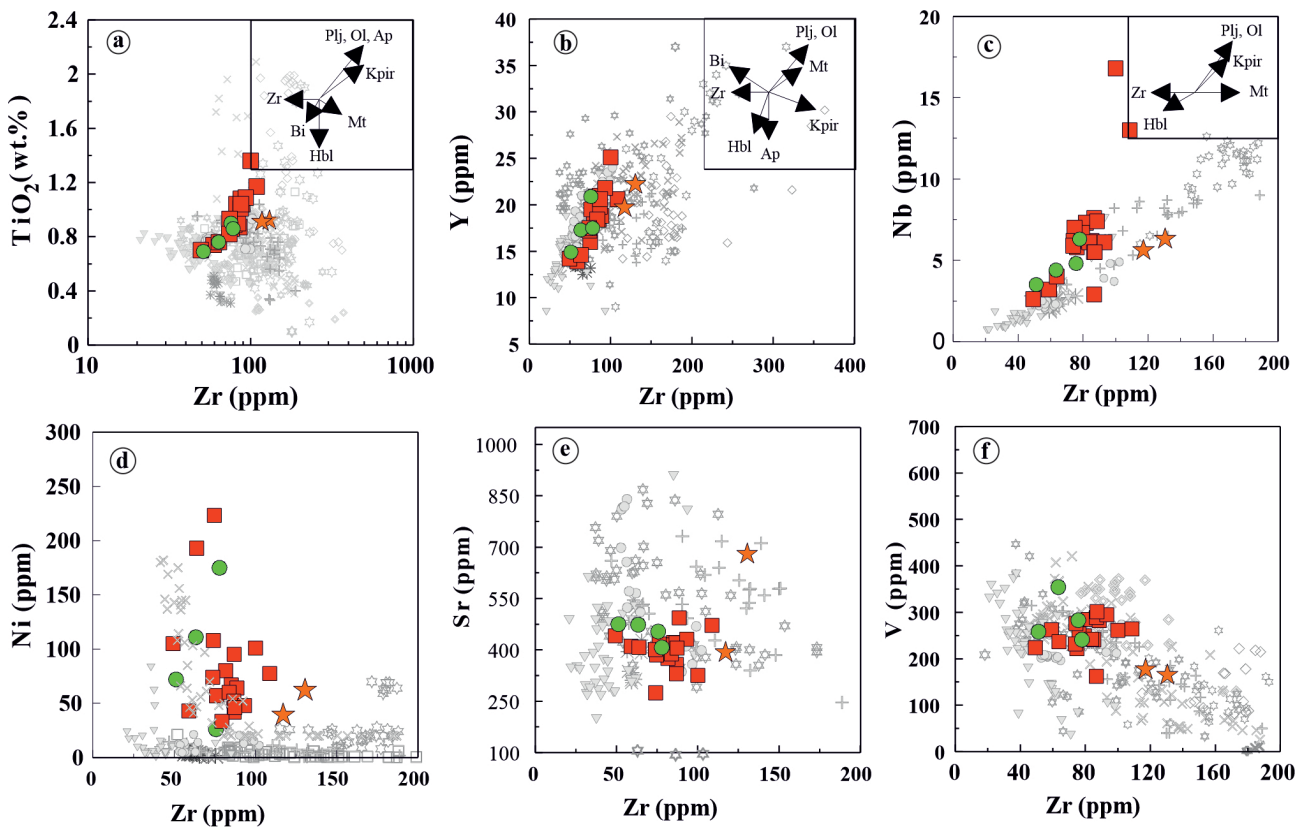


**Figure 11.** Zr (ppm) versus  $\text{TiO}_2$  (wt. %), Y (ppm), Nb (ppm), Ni (ppm), Sr (ppm) and V (ppm) diagrams demonstrating the fractional crystallization (FC) and accumulation of the Narman volcanic rocks (vectors show fractional crystallization and accumulation, according to Pearce and Norry (1979), symbols are as in Figure 4). Data sources for comparison of other Eocene volcanic rocks are as in Figure 7d.

plagioclase fractionation (Figure 11e). The clear negative trends on the diagram for Zr versus the compatible element V (Figure 11f) indicate Fe-Ti oxide fractionation.

The trends in the vertical direction on the Nb/Y versus Rb/Y diagram for the studied volcanic rocks suggest subduction zone enrichment and/or crustal contamination occurred, while positive trends around  $\text{Rb}/\text{Nb} = 1$  and high Nb/Y values indicate within-plate enrichment. For the samples of the Narman Volcanics, subduction enrichment, crustal assimilation, and within-plate enrichment played an effective role (Figure 12).

To determine the role of fractionation and crustal assimilation in samples from the Narman volcanic rocks, the  $\text{SiO}_2$  versus Sr and Nd isotope ratios and Th diagrams were drawn (Figures 13a–13d). Positive and negative trends indicate that magma was affected by crustal assimilation with fractional crystallization (AFC) processes, while a flat trend shows that fractionation was effective. According to the variation diagrams, fractional crystallization (FC) and/or AFC are suggested by changes in primitive source fields. The variations occurring in horizontal and close to horizontal directions in Figures 13a–13d indicate FC,

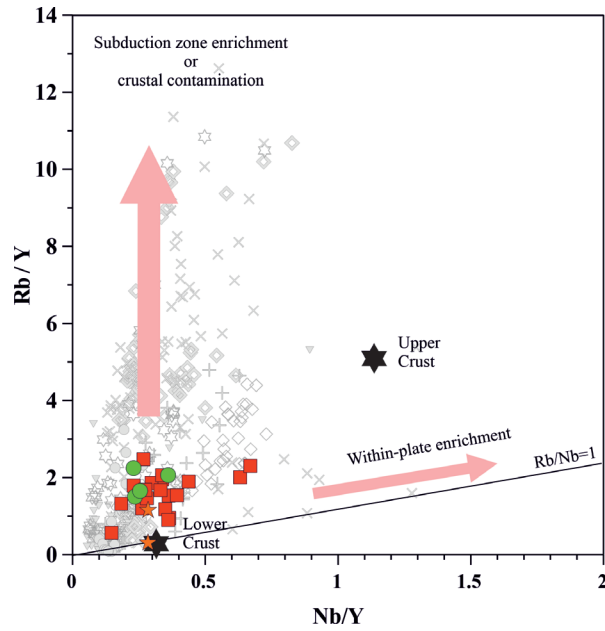


**Figure 12.** Nb/Y versus Rb/Y plots of the Narman Volcanites (diagram are taken from Pearce et al., 1990; compositions of the upper and lower crusts after Taylor and McLennan, 1985) (symbols are as in Figure 4). Data sources for comparison of other Eocene volcanic rocks are as in Figure 7d.

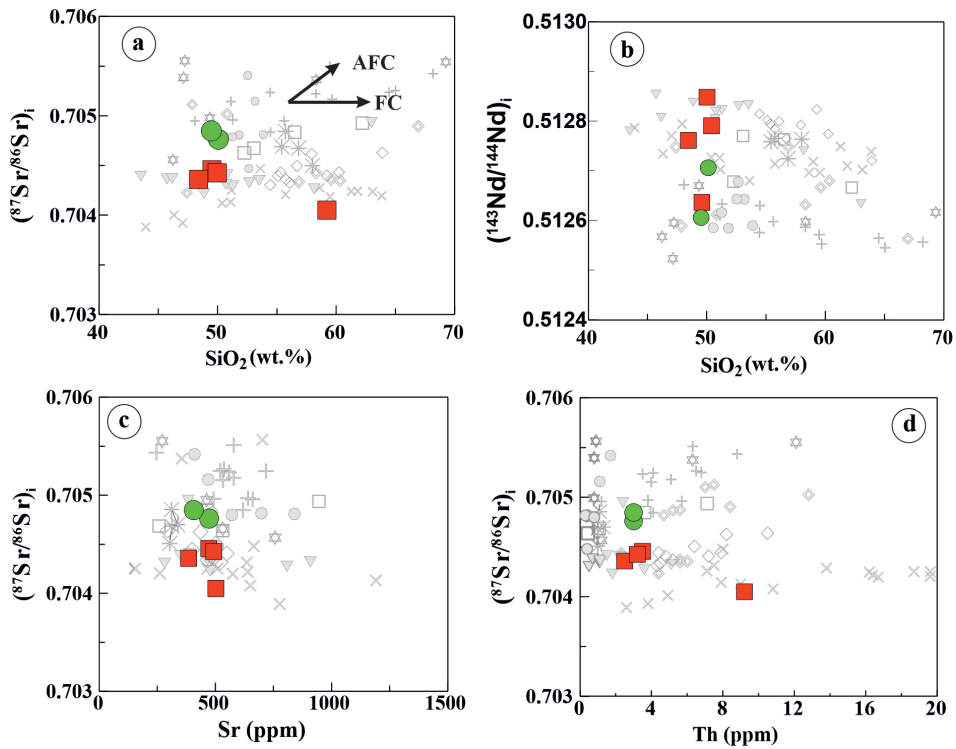


**Figure 13.** (a)  $\text{SiO}_2$  versus  $(^{87}\text{Sr}/^{86}\text{Sr})_i$ , (b)  $\text{SiO}_2$  versus  $(^{143}\text{Nd}/^{144}\text{Nd})_i$ , (c) Sr versus  $(^{87}\text{Sr}/^{86}\text{Sr})_i$ , and (d) Th versus  $(^{87}\text{Sr}/^{86}\text{Sr})_i$  plots showing possible fractional crystallization (FC) and/or assimilation-fractional crystallization (AFC) trends for the Narman volcanic rocks (symbols are as in Figure 4). Data sources for comparison of other Eocene volcanic rocks are as in Figure 7d.

while positive or negative trends indicate AFC. During the formation of the basaltic dyke and basaltic lava rocks comprising the Narman volcanic rocks, AFC can be generally said to play a more effective role.

### 5.3. Source nature

The trace element variation diagrams for the Narman volcanic rocks have features of typical subduction zone volcanic rocks with depletion of HFSE elements such as Nb, Zr, and Ta, enrichment of LILE such as Sr, K, Rb, and Ba, and high Ba/La ratios (Figures 8a–8d; Ewart, 1982; Pearce, 1983).

As is known, enrichment in HFSE compared to LILE, enrichment in HREE compared to LREE and negative Nb, Ta, Zr, Hf, and Ti anomalies are characteristic of subduction-related continental arc magmas (McCulloch and Gamble, 1991; Thirlwall et al., 1994; Kelemen et al., 2003). Contrarily, the presence of positive Nb, Ta, and Ti anomalies (Figures 9a–9d) differentiates ocean island basalts (OIB) from subduction zone arc volcanics (Hofmann, 1997). Enrichments in LILE and LREE (Figures 9a–9h) show that the main magma was derived from a source region (probably lithospheric mantle) enriched by fluids emerging from subducting oceanic lithosphere and/or sediments on the subducting lithosphere (metasomatism) (Cameron et al., 2003; Münker et al., 2004). On the Sr/Th versus  $^{87}\text{Sr}/^{86}\text{Sr}$  diagram (Figure 14a), high Sr/Th ratio indicates fluid phases. The Sr isotope ratio varies depending on whether there is interaction with altered basaltic crust ( $\geq 0.704$ ; Bickle and Teagle, 1992; Staudigel et al., 1995) with fluids or with subducting sediments ( $> 0.709$ ).

Hawkesworth et al. (1997) stated that rocks with high Sr/Th ratio and low  $^{87}\text{Sr}/^{86}\text{Sr}$  (approximately 0.704) value develop in several volcanic arcs based on the correlation of  $^{87}\text{Sr}/^{86}\text{Sr}$  versus Sr/Th. Based on this, low  $^{87}\text{Sr}/^{86}\text{Sr}$  value was proposed to support fluid composition while high  $^{87}\text{Sr}/^{86}\text{Sr}$  value was proposed to support sediment composition. The  $^{87}\text{Sr}/^{86}\text{Sr}$  versus Sr/Th diagram for rocks in depleted and enriched arcs have a trend with hyperbolic shape (Figure 14a). The Narman volcanic rocks are like rocks forming in depleted arcs with low Sr/Th ( $< 200$ ) ratio and low  $^{87}\text{Sr}/^{86}\text{Sr}$  ( $< 0.705$ ) value (Macdonald et al., 2000). Again, the Ba/La versus Th/Yb diagram is used to show fluid or sediment input in subduction zones (Figure 14b). The vertical trend on the diagram indicates mantle enriched by metasomatism with subducting fluids, while the horizontal trend indicates mantle source enriched by metasomatism related to subducting sediments. The basaltic dyke, basaltic lava, and basaltic volcanic breccia samples from the Narman Volcanics display enrichment trends associated with fluids (Figure 14b). The Ta/Yb versus Th/Yb diagram (Figure 14c) provides the opportunity to interpret whether variations in source composition and crustal contamination were

effective in evolution of magma or not. The vertical trend toward higher Th/Yb ratios on this diagram (Figure 14c) shows the effect of subduction-derived fluids and/or melts, while high Th/Yb and parallel or subparallel trends to the mantle series show FC and AFC. As seen on this diagram, fractionation in addition to crustal assimilation appears to be effective on the evolution of the Eocene volcanic rocks.

According to Smith et al. (1999), the lithospheric mantle is more depleted in LREE compared to HFSE (such as Nb and Ta). The high Nb/La ratio (approximately  $> 1$ ) for basaltic magma shows an asthenospheric mantle source, while a low ratio (approximately  $> 0.5$ ) shows a lithospheric mantle source. The most basic samples from the Narman volcanic rocks had Nb/La ratio from 0.29 to 0.70, while the La/Yb ratio ranged from 4.26 to 17.14, and these values indicate lithospheric mantle source (Figure 14d).

Petrological models based on trace element content may be used to determine source mineralogy, scope, depth, and degree of partial melt. Shaw (1970) proposed a model to determine the mineralogic and geochemical composition of the source area and partial melt conditions for magmas. The almost flat HREE patterns for the studied volcanic rock samples indicate mantle mineralogy containing spinel, probably shallower than 85 km (McKenzie and O'Nions, 1991; Klemme, 2004). Mantle mineralogy containing garnet, indicating a deeper source generally, produces melts with higher  $\text{Dy}/\text{Yb}_N$  ratios ( $> 2.5$ , Yang et al., 2012), while a source containing spinel has lower  $\text{Dy}/\text{Yb}_N$  ratios ( $< 1.5$ ). The  $\text{Dy}/\text{Yb}$  ratios for basaltic dyke, basaltic lava, and basaltic volcanic breccia samples from the Narman volcanic rocks vary from 1.15 to 1.30, 1.22 to 2.27, and 1.08 to 1.47, respectively. To estimate the source mineralogy and degree of partial melting,  $\text{La}/\text{Yb}_N$  versus  $\text{Dy}/\text{Yb}_N$  and Th versus  $(\text{Tb}/\text{Yb})_N$  are used (Figures 14e and 14f). The  $\text{Dy}/\text{Yb}_N$  ratios of the studied rocks are similar to other Eocene volcanic rocks in the EPOB, indicating that mostly melting of spinel peridotite (approximately 1-3 partial melt) could produce the melts for the Narman volcanic rocks.

### 5.4. Geodynamic implications

Tertiary volcanic rocks in the Eastern Pontides have been investigated by several researchers and much data was obtained about the evolution of Tertiary volcanism because of these investigations. This study for the Eocene volcanic rocks from the Narman area was compared with other studies of volcanics outcropping in the Eastern Pontides to collate information about the evolution of Tertiary volcanism in the region. Middle Eocene volcanic and sedimentary units commonly outcrop in the Central Pontides in Hamamözü (Amasya), Almus (Tokat) and Yıldızeli (Sivas) and in the Eastern Pontides in Artvin and

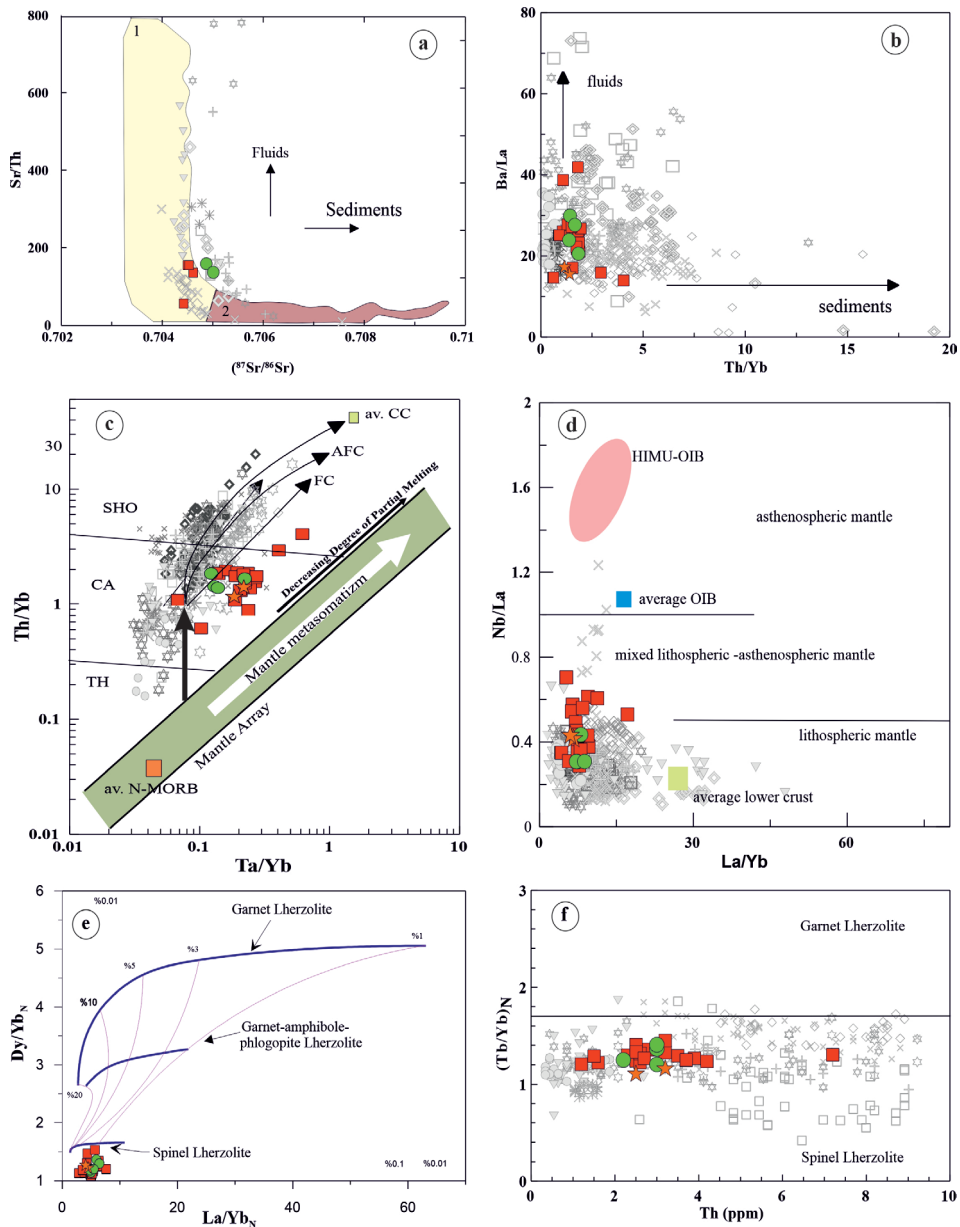


**Figure 14.** (a)  $^{87}\text{Sr}/^{86}\text{Sr}$  versus  $\text{Sr}/\text{Th}$  variations in Narman volcanic rocks. Fields 1 and 2 enclose data from arcs considered incompatible element depleted and enriched, respectively, by Hawkesworth et al. (1997). The arrows show the sense of enrichment predicted from addition of fluid and sedimentary components to the mantle wedge, (b)  $\text{Th}/\text{Yb}$  versus  $\text{Ba}/\text{La}$  diagram (Woodhead et al., 2001), (c)  $\text{Th}/\text{Yb}$  versus  $\text{Ta}/\text{Yb}$  diagram (after Pearce et al., 1990) for the Narman Volcanics. Average N-MORB composition and average CC (Continental Crust) are from Sun and McDonough (1989) and Taylor and McLennan (1985), respectively. Vectors showing inferred effects of fractional crystallization (FC), assimilation-fractional crystallization (AFC), subduction enrichment and mantle metasomatism are from Pearce et al. (1990), (d)  $\text{La}/\text{Yb}$  versus  $\text{Nb}/\text{La}$  diagrams for Narman Volcanics. Dashed lines separating fields of the asthenospheric, lithospheric and mixed mantle are plotted based on data given in Smith et al. (1999), the HIMU-OIB area is reported in Weaver et al. (1987), (e)  $\text{Dy}/\text{Yb}_N$  versus  $\text{La}/\text{Yb}_N$  nonmodal batch melting curves were calculated by using partition coefficients from Rollinson (1993), McKenzie and O’Nions (1991) and Keskin (2002), (f)  $\text{Th}$  (ppm) versus  $\text{Tb}_N/\text{Yb}_N$  horizontal line separates fields expected for melting garnet- and spinel-lherzolite as determined for Basin and Range basalts (Wang et al., 2002), (symbols are as in Figure 4). Data sources for comparison of other Eocene volcanic rocks are as in Figure 7d.

Narman (Erzurum) (Keskin et al., 2008; Arslan et al., 2013; Yücel et al., 2017; Göçmengil et al., 2018, 2022; Aydınçakır et al., 2022). Considering detailed geochronological and geochemical studies, the geodynamic evolution of the Eastern Pontides was considered a paleo-arc environment by numerous authors. Though much data has been produced using modern analytical techniques in recent years, debates related to the geodynamic evolution of the region continue and a final model has still not been developed. Though debates focus on studies related more to subduction polarity, timing of collision and postcollisional events, the following geodynamic models were proposed; (1) slab breakoff model (Altunkaynak, 2007; Keskin et al., 2008; Dokuz et al., 2019), (2) delamination model in a north-dipping subduction system (Dilek et al., 2010; Arslan et al., 2013; Temizel et al., 2012, 2016; Aydınçakır and Şen, 2013; Kaygusuz et al., 2020, 2022; Aydınçakır et al., 2022), and (3) ridge subduction model in a south-dipping subduction system (Eyuboglu et al., 2011, 2016). Despite contrasting beliefs about the geodynamic evolution of the Eastern Pontides, most researchers have reached consensus that the region evolved through consecutive crustal thickening and collisional processes with an initial north-dipping subduction zone (Şengör and Yılmaz, 1981; Yılmaz et al., 1997; Okay and Sahinturk, 1997; Boztuğ et al., 2004). Though the slab breakoff model was proposed as an applicable model to explain the narrow Middle Eocene volcanism along the İzmir–Ankara–Erzincan Suture Zone (İAESZ) in the Central Pontides, the applicability of the lithospheric delamination model is accepted to explain the common Middle Eocene volcanism in the north of the Eastern Pontides. Additionally, the Eastern Pontides were affected by postcollisional extensional collapse with delamination. During the middle Eocene, widespread magmatism developed along the entire range of the İAESZ, from the western to eastern parts of Türkiye (Yılmaz et al., 1997; Keskin et al., 2008). The Eastern Pontides was associated with slab breakoff with adakitic dominant magmatism on very localized scales in the Early Eocene (57–47 My; Karsli et al., 2011; Dokuz et al., 2013). Middle Eocene volcanic units are more common compared to Early Eocene magmatic units. Additionally, a geodynamic tectonomagmatic event on lithospheric scale (delamination and/or lithospheric removal) appears to be much more reasonable than a local tectonomagmatic event (slab breakoff) due to the distribution of similar units in different sections of the Central and Eastern Pontides (Keskin et al., 2008; Arslan et al., 2013; Göçmengil et al., 2018; Aydınçakır et al., 2022). The lack of high-pressure metamorphism along the crustal blocks in the south section and surroundings of the Pontides during the Eocene means that the probability of subduction-related magmatism is not possible for the investigated

units. Mixing of mantle previously metasomatized by subduction-related solutions and lower continental crust source magmas caused the Middle Eocene magmatism (Yılmaz and Boztuğ, 1996). The geodynamic evolution of Middle Eocene magmatism along the Eastern Pontides is best explained by the delamination model, as supported by the data obtained during this research. The formation of partial melts for Middle Eocene magmatism in the Eastern Pontides may be explained by geothermal perturbation subsequent to asthenospheric elevation linked to fragmented and asymmetrical delamination (Arslan et al., 2013, 2022; Temizel et al., 2016; Yücel et al., 2017). The E-W, NE-SW, and NW-SE strike-slip movements controlling the neotectonic evolution of the Eastern Pontides contributed to the block-fault architecture of the region and formed important extensional tectonic structures in the region (Bektaş and Çapkınoğlu, 1997; Maden et al., 2009; Öztürk and Kaya, 2019). Extensional tectonics probably assisted in reducing pressure in uppercrust magma chambers. Extension related to lithospheric delamination controlling regional strike-slip movements in the postcollisional environment caused asthenospheric upwelling. Similar extensional tectonics may trigger delamination and lithospheric uplift processes in several regions around the world (Ducea et al., 2013). Decompression and sudden disruption at uppercrustal levels probably reactivated partially melted magma and caused the development of fractional crystallization along with some crustal assimilation (AFC) processes in the region. The whole-rock geochemistry and isotopic characteristics of volcanic rocks in the Narman region show that the magma source for these rocks formed in a postcollisional extensional geodynamic environment because of partial melting of lithospheric mantle previously metasomatized by fluids with subduction composition.

## 6. Conclusion

- (1) The Narman volcanic rocks are divided into basic dyke, basaltic lava, and basaltic volcanic breccia facies. The volcanic rocks contain plagioclase ( $An_{34-80}$ ), clinopyroxene ( $Wo_{38-47}En_{41-50}Fs_{5-18}$ ), and olivine ( $Fo_{68-90}$ ) phenocrystals with magnetite/titanomagnetite.
- (2)  $^{40}Ar-^{39}Ar$  plateau ages range from  $44.5 \pm 0.1$  Ma to  $43.4 \pm 0.1$  Ma for the studied volcanic rock samples and the period of the postcollisional extensional regime in the EPOB.
- (3) Positive and negative correlations observed on variation diagrams show that fractional crystallization was very effective during the evolution of the rocks. Harker diagrams show clinopyroxene + plagioclase + olivine  $\pm$  magnetite fractionation played important roles in the development of the rocks.

(4) The plotting of Sr-Nd-Pb-Hf isotope values from all samples close to the mantle interval indicates the Narman volcanic rocks derived from an isotopically depleted mantle source.

(5) Considering the petrographic, geochemical and petrological features and isotopic data for volcanic rocks from the Narman region, an attempt was made to model magmatic processes during the evolution of the volcanic rocks. The modeling results indicate with high probability that the magma is derived from the partial melting of a mantle source that experienced metasomatism by subduction fluids (enriched) and later evolved through magmatic events such as fractionation  $\pm$  assimilation in shallow magma chambers within the continental crust.

## References

- Altunkaynak Ş (2007). Collision-driven slab breakoff magmatism in northwestern Anatolia, Turkey. *The Journal of Geology* 115 (1): 63-82. <https://doi.org/10.1086/509268>
- Arslan M, Temizel İ, Abdioğlu E, Kolaylı H, Yücel C et al. (2013). 40Ar-39Ar dating, whole-rock and Sr-Nd-Pb isotope geochemistry of post-collisional Eocene volcanic rocks in the southern part of the Eastern Pontides (NE Turkey): implications for magma evolution in extension-induced origin. *Contributions to Mineralogy and Petrology* 166: 113-142. <https://doi.org/10.1007/s00410-013-0868-3>
- Arslan M, Temizel İ, Ackerman L, Yücel C, Abdioğlu Yazar E (2022). Highly siderophile element and Os isotope systematics of the Cenozoic volcanic rocks from the Eastern Pontides, NE Turkey: constraints on the origin and evolution of subcontinental mantle-derived magmas. *Lithos* 410-411: 106575. <https://doi.org/10.1016/j.lithos.2021.106575>
- Aslan Z, Arslan M, Temizel İ, Kaygusuz A (2014). K-Ar dating, whole-rock and Sr-Nd isotope geochemistry of calcalkaline volcanic rocks around the Gümüşhane area: implications for post-collisional volcanism in the Eastern Pontides, Northeast Turkey. *Mineralogy and Petrology* 108: 245-267. <https://doi.org/10.1007/s00710-013-0294-2>
- Aydin F, Oğuz Saka S, Şen C, Dokuz A, Aiglsperger T et al. (2020). Temporal, geochemical and geodynamic evolution of the Late Cretaceous subduction zone volcanism in the eastern Sakarya Zone, NE Turkey: implications for mantle-crust interaction in an arc setting. *Journal of Asian Earth Science* 192: 1-23. <https://doi.org/10.1016/j.jseas.2019.104217>
- Aydınçakır E, Şen C (2013). Petrogenesis of the post-collisional volcanic rocks from the Borçka (Artvin) area: implications for the evolution of the Eocene magmatism in the Eastern Pontides (NE Turkey). *Lithos* 172-173: 98-117. <https://doi.org/10.1016/j.lithos.2013.04.007>
- Aydınçakır E (2014). The petrogenesis of Early Eocene non-adakitic volcanism in NE Turkey: constraints on the geodynamic implications: *Lithos* 208-209: 361-377. <https://doi.org/10.1016/j.lithos.2014.08.019>
- Aydınçakır E (2016). Subduction-related Late Cretaceous high-K volcanism in the Central Pontides orogenic belt: constraints on geodynamic implications. *Geodinamica Acta* 28 (4): 379-411. <https://doi.org/10.1080/09853111.2016.1208526>
- Aydınçakır E, Gündüz R, Yücel C (2020). Emplacement conditions of magma(s) forming Jurassic plutonic rocks in Gümüşhane (Eastern Pontides, Turkey). *Bulletin of the Mineral Research and Exploration* 162: 175-196. <https://doi.org/10.19111/bulletinofmre.649808>
- Aydınçakır E, Yücel C, Ruffet G, Gücer MA, Akaryalı E et al. (2022). Petrogenesis of post-collisional Middle Eocene volcanism in the Eastern Pontides (NE, Turkey): insights from geochemistry, whole-rock Sr-Nd-Pb isotopes, zircon U-Pb and 40Ar-39Ar geochronology. *Geochemistry* 82 (2): 125871. <https://doi.org/10.1016/j.chemer.2022.125871>
- Aydınçakır E, Yücel C, Kaygusuz A, Bilici Ö, Yi K et al. (2023). Magmatic evolution of the Calc-alkaline Middle Jurassic igneous rocks in the eastern pontides, NE Turkey: insights from geochemistry, whole-rock Sr-Nd-Pb, in situ zircon Lu-Hf isotopes, and U-Pb geochronology. *International Geology Review* 65 (20): 3146-3167. <https://doi.org/10.1080/00206814.2023.2177890>
- Bacon CR, Hirschmann MM (1988). Mg/Mn partitioning as a test for equilibrium between coexisting Fe-Ti oxides. *American Mineralogist* 73 (1-2): 57-61.
- Bayraktutan S (1994). Narman-Gaziler Bölgesinin Tersiyer'deki Volkano-Tektonik Evrimi: 47. *Türkiye Jeoloji Kurultayı, Bildiri Özleri* (in Turkish).
- Bektaş O, Çapkınoğlu Ş (1997). Doğu pontid magmatik arkında (KD, Türkiye) neptünyen dayklar ve blok tektoniği. *Geosound* 30: 451-463.
- Benda L (1971). Grundzüge einer pollenanalytischen gliederung des Türkischen Jungtertiärs. *Beihefte zum Geologischen Jahrbuch* 113 (in German).



- Bickle MJ, Teagle DAH (1992). Strontium alteration in the Troodos ophiolite: implications for fluid fluxes and geochemical transport in mid-ocean ridge hydrothermal systems. *Earth and Planetary Sciences Letters* 113 (1-2): 219-237. [https://doi.org/10.1016/0012-821X\(92\)90221-G](https://doi.org/10.1016/0012-821X(92)90221-G)
- Boztuğ D, Jonckheere RC, Wagner GA, Yeğingil Z (2004). Slow Senonian and fast Paleocene-early Eocene uplift of the granitoids in the Central Eastern Pontides, Turkey: apatite fission-track results. *Tectonophysics* 382 (3-4): 213-228. <https://doi.org/10.1016/j.tecto.2004.01.001>
- Buket E, Temel A (1998). Major-element, trace-element, and Sr-Nd isotopic geochemistry and genesis of Varto (Muş) volcanic rocks, Eastern Turkey. *Journal of Volcanology and Geothermal Research* 85 (1-4): 405-422. [https://doi.org/10.1016/S0377-0273\(98\)00064-X](https://doi.org/10.1016/S0377-0273(98)00064-X)
- Cameron BI, Walker JA, Carr MJ, Patino LC, Matias O et al. (2003). Flux versus decompression melting at stratovolcanos in southeastern Guatemala. *Journal of Volcanology Geothermal Research* 119 (1-4): 21-50. [https://doi.org/10.1016/S0377-0273\(02\)00304-9](https://doi.org/10.1016/S0377-0273(02)00304-9)
- Chauvel C, Blichert-Toft J (2001). A hafnium and trace element perspective on melting of the depleted mantle. *Earth and Planetary Sciences Letters* 190 (3-4): 137-151. [https://doi.org/10.1016/S0012-821X\(01\)00379-X](https://doi.org/10.1016/S0012-821X(01)00379-X)
- Condie KC, Frey BA, Kerrich R (2002). The 1.75-Ga Iron King Volcanics in west-central Arizona: a remnant of an accreted oceanic plateau derived from a mantle plume with a deep depleted component. *Lithos* 64 (1-2): 49-62. [https://doi.org/10.1016/S0024-4937\(02\)00158-5](https://doi.org/10.1016/S0024-4937(02)00158-5)
- Davies JH, von Blanckenburg F (1995). Slab breakoff: a model of lithospheric detachment and its test in the magmatism and deformation of collisional orogens. *Earth and Planetary Science Letters* 129 (1-4): 85-102. [https://doi.org/10.1016/0012-821X\(94\)00237-S](https://doi.org/10.1016/0012-821X(94)00237-S)
- Dewey JF, Pitman WC, Ryan WBF, Bonnin J (1973). Plate tectonics and the evolution of the Alpine system. *Geological Society of American Bulletin* 84: 3137-3180. [https://doi.org/10.1130/0016-7606\(1973\)84<3137:PTATEO>2.0.CO;2](https://doi.org/10.1130/0016-7606(1973)84<3137:PTATEO>2.0.CO;2)
- Dilek Y, Imamverdiyev N, Altunkaynak Ş (2010). Geochemistry and tectonics of Cenozoic volcanism in the Lesser Caucasus (Azerbaijan) and the peri-Arabian region: Collision-induced mantle dynamics and its magmatic fingerprint. *International Geology Review* 52 (4-6): 536-578. <https://doi.org/10.1080/00206810903360422>
- Dokuz A (2011). A slab detachment and delamination model for the generation of Carboniferous high-potassium I type magmatism in the Eastern Pontides, NE Turkey: the Köse composite pluton. *Gondwana Research* 19 (4): 926-944. <https://doi.org/10.1016/j.gr.2010.09.006>
- Dokuz A, Uysal İ, Siebel W, Turan M, Duncan R et al. (2013). Post-collisional adakitic volcanism in the eastern part of the Sakarya Zone, Turkey: evidence for slab and crustal melting. *Contributions to Mineralogy and Petrology* 166: 1443-1468. <https://doi.org/10.1007/s00410-013-0936-8>
- Dokuz A, Aydınçakır E, Kandemir R, Karşlı O, Siebel W et al. (2017). Late Jurassic magmatism and stratigraphy in the Eastern Sakarya zone, Turkey: evidence for the slab breakoff of Paleotethyan oceanic lithosphere. *The Journal of Geology* 125: 1-3. <https://doi.org/10.1086/689552>
- Dokuz A, Aydın F, Karşlı O (2019). Post-collisional transition from subduction- to intraplate-type magmatism in the eastern Sakarya zone, Turkey: indicators of northern Neotethyan slab breakoff. *The Geological Society of America Bulletin* 131 (9-10): 1623-1642. <https://doi.org/10.1130/B31993.1>
- Dokuz A, Gücer MA, Karşlı O, Yi K (2022). From Cadomian back-arc basin to Rheic Ocean closure: the geochronological records of the Kurtoğlu Massif, eastern Sakarya Zone, Turkey. *International Journal of Earth Science* 111: 1333-1355. <https://doi.org/10.1007/s00531-022-02183-4>
- Ersoy EY, Palmer MR, Genç ŞC, Prelević D, Akal C et al. (2017). Chemo-probe into the mantle origin of the NW Anatolia Eocene to Miocene volcanic rocks: implications for the role of, crustal accretion, subduction, slab roll-back and slab break-off processes in genesis of post-collisional magmatism. *Lithos* 288-289: 55-71. <https://doi.org/10.1016/j.lithos.2017.07.006>
- Eyuboglu Y, Santosh M, Chung S-L (2011). Petrochemistry and U-Pb zircon ages of adakitic intrusions from the Pular Massif (Eastern Pontides, NE Turkey): implications for slab rollback and ridge subduction associated with Cenozoic convergent tectonics in the Eastern Mediterranean. *The Journal of Geology* 119: 394-417. <https://doi.org/10.1086/660158>
- Eyuboglu Y, Santosh M, Yi K, Bektaş O, Kwon S (2012). Discovery of Miocene adakitic dacite from the Eastern Pontides Belt (NE Turkey) and a revised geodynamic model for the late Cenozoic evolution of Eastern Mediterranean region. *Lithos* 146-147: 218-232. <https://doi.org/10.1016/j.lithos.2012.04.034>
- Eyuboglu Y, Dudas FO, Santosh M, Zhu DC, Yi K et al. (2016). Cenozoic forearc gabbros from the northern zone of the Eastern Pontides Orogenic Belt, NE Turkey: implications for slab window magmatism and convergent margin tectonics. *Gondwana Research* 33: 160-190. <https://doi.org/10.1016/j.jgr.2015.07.006>
- Ewart A (1982). The mineralogy and petrology of Tertiary-Recent orogenic volcanic rocks: with special reference to the andesitic-basaltic compositional range. In Thorpe RS (editor). *Andesites: Orogenic Andesites and Related Rocks*. Chichester, UK: J. Wiley and Sons, pp. 25-95.
- Gill JB (1981). *Orogenic Andesites and Plate Tectonics*. Berlin, Germany: Springer.
- Göçmengil G, Karacık Z, Genç ŞC, Billor MZ (2018). <sup>40</sup>Ar-<sup>39</sup>Ar geochronology and petrogenesis of post-collisional trachytic volcanism along the İzmir-Ankara-Erzincan suture zone (NE, Turkey). *Turkish Journal of Earth Sciences* 27 (1): 1-31. <https://doi.org/10.3906/yer-1708-4>
- Göçmengil G; Karacık Z; Genç ŞC, Prelević D, Billor Z (2019). <sup>40</sup>Ar-<sup>39</sup>Ar ages and petrogenesis of middle Eocene post-collisional volcanic rocks along the İzmir-Ankara-Erzincan suture zone, NE Turkey. *Journal of Asian Earth Science* 173: 121-142. <https://doi.org/10.1016/j.jseas.2019.01.001>

- Göçmengil G, Gülmez F, Karacık Z, Aysal N (2022). Petrogenesis of Early Cenozoic Sarıcakaya–Nallıhan Volcanism in NW Turkey: implications for the geodynamic setting and source characterization of the Balkanatolia Magmatic Realm. *Minerals* 12; 1572. <https://doi.org/10.3390/min12121572>
- Gücer MA (2021). Origin, petrogenesis and geodynamic implications of the early Eocene Altınpınar adakitic andesites in the eastern Sakarya Zone, northeastern Turkey. *Geochemistry* 81 (2): 125766. <https://doi.org/10.1016/j.chemer.2021.125766>
- Gülmez F, Genç ŞC, Keskin M, Tüysüz O (2013). A post-collision slab-breakoff model for the origin of the Middle Eocene magmatic rocks of the Armutlu-Almacık belt, NW Turkey and its regional implications. *Geological Society, London, Special Publications* 372 (1): 107–139. <https://doi.org/10.1144/SP372.12>
- Hawkesworth CJ, Turner SP, McDermott F, Peate DW, van Calsteren P (1997). U-Th isotopes in arc magmas: implications for element transfer from the subducted crust. *Science* 276 (5312): 551-555. <https://doi.org/10.1126/science.276.5312.551>
- Hofmann AW (1997). Mantle geochemistry: the message from oceanic volcanism. *Nature* 385: 219-229. <https://doi.org/10.1038/385219a0>
- Irvine TN, Baragar WRA (1971). A Guide Chemical Classification of The Common Volcanic Rock, *Canadian Journal of Earth Science* 8: 523-548. <https://doi.org/10.1139/e71-055>
- Jacobsen SB, Wasserburg GJ (1980). Sm–Nd isotopic evolution of chondrites. *Earth and Planetary Science Letters* 50 (1): 139-155. [https://doi.org/10.1016/0012-821X\(80\)90125-9](https://doi.org/10.1016/0012-821X(80)90125-9)
- Kandemir R, Yılmaz C (2009). Lithostratigraphy, facies, and deposition environment of the lower Jurassic Ammonitico Rosso type sediments (ARTS) in the Gümüşhane, area, NE Turkey: implications for the opening of the northern branch of the NeoTethys Ocean. *Journal of Asian Earth Sciences* 34 (4): 586-598. <https://doi.org/10.1016/j.jseaes.2008.08.006>
- Karsli O, Chen B, Uysal I, Aydın F, Wijbrans JR et al. (2008). Elemental and Sr–Nd–Pb isotopic geochemistry of the most recent Quaternary volcanism in the Erzincan Basin, Eastern Turkey: framework for the evaluation of basalt–lower crust interaction. *Lithos* 106 (1-2): 55-70. <https://doi.org/10.1016/j.lithos.2008.06.008>
- Karsli O, Ketenci M, Uysal İ, Dokuz A, Aydın F et al. (2011). Adakite-like granitoid porphyries in Eastern Pontides, NE Turkey: potential parental melts and geodynamic implications. *Lithos* 127 (1-2): 354-372. <https://doi.org/10.1016/j.lithos.2011.08.014>
- Karsli O, Dokuz A, Uysal İ, Ketenci M, Chen B et al. (2012). Deciphering the shoshonitic monzonites with I-type characteristic, the Sıldağı pluton, NE Turkey: magmatic response to continental lithospheric thinning. *Journal of Asian Earth Science* 51: 45–62. <https://doi.org/10.1016/j.jseaes.2012.02.003>
- Karsli O, Dokuz A, Kandemir R (2017). Zircon Lu–Hf isotope systematics and U–Pb geochronology whole-rock Sr–Nd isotopes and geochemistry of the early Jurassic Gokcedere pluton, Sakarya Zone–NE Turkey: a magmatic response to roll-back of the Paleotethyan oceanic lithosphere. *Contributions to Mineralogy and Petrology* 172: 1–31. <https://doi.org/10.1007/s00410-017-1346-0>
- Karsli O, Şengün F, Dokuz A, Kandemir R, Aydın F et al. (2020a). Silurian to early Devonian arc magmatism in the western Sakarya Zone (NW Turkey) with inference to the closure of the Rheic Ocean. *Lithos* 370-371: 105641. <https://doi.org/10.1016/j.lithos.2020.105641>
- Karsli O, Caran Ş, Çoban H, Şengün F, Tekkanat O et al. (2020b). Melting of the juvenile lower crust in a far-field response to roll-back of the southern Neotethyan oceanic lithosphere: the Oligocene adakitic dacites, NE Turkey. *Lithos* 370-371: 105614. <https://doi.org/10.1016/j.lithos.2020.105614>
- Kaygusuz A (2009). K/Ar ages and geochemistry of the collision related volcanic rocks in the İllca (Erzurum) area, eastern Turkey. *Neues Jahrbuch für Mineralogie - Abhandlungen* 186 (1): 21-36. <https://doi.org/10.1127/0077-7757/2009/0134>
- Kaygusuz A, Aydınçakır E (2009). Mineralogy, whole rock and Sr–Nd isotope geochemistry of mafic microgranular enclaves in Cretaceous Dagbasi granitoids, Eastern Pontides, NE Turkey: evidence of magma mixing, mingling, and chemical equilibration. *Geochemistry* 69 (3): 247-277. <https://doi.org/10.1016/j.chemer.2008.08.002>
- Kaygusuz A, Arslan M, Siebel W, Sipahi F, İlbeli N (2012). Geochronological evidence and tectonic significance of Carboniferous magmatism in the southwest Trabzon area, Eastern Pontides, Turkey. *International Geology Review* 54: 1776-1800. <https://doi.org/10.1080/00206814.2012.676371>
- Kaygusuz A, Aslan Z, Aydınçakır E, Yücel C, Gücer MA et al. (2018). Geochemical and Sr–Nd–Pb isotope characteristics of the Miocene to Pliocene volcanic rocks from the Kandilli (Erzurum) area, Eastern Anatolia (Turkey): implications for magma evolution in extension-related origin. *Lithos* 296-299: 332-351. <https://doi.org/10.1016/j.lithos.2017.11.003>
- Kaygusuz A, Yücel C, Arslan M, Temizel İ, Yi K et al. (2020). Eocene I-type magmatism in the Eastern Pontides, NE Turkey: insights into magma genesis and magma-tectonic evolution from whole-rock geochemistry, geochronology and isotope systematics. *International Geology Review* 62 (11): 1406-1432. <https://doi.org/10.1080/00206814.2019.1647468>
- Kaygusuz A, Arslan M, Temizel İ, Yücel C, Aydınçakır E (2021). U–Pb zircon ages and petrogenesis of the Late Cretaceous I-type granitoids in arc setting Eastern Pontides, NE Turkey. *Journal of African Earth Sciences* 174: 104040. <https://doi.org/10.1016/j.jafrearsci.2020.104040>
- Kaygusuz A, Yücel C, Aydınçakır E, Gücer MA, Ruffet G (2022). 40Ar–39Ar dating, whole-rock and Sr–Nd isotope geochemistry of the Middle Eocene calc-alkaline volcanic rocks in the Bayburt area Eastern Pontides (NE Turkey): implications for magma evolution in extension-related setting. *Mineralogy and Petrology* 116: 379-399. <https://doi.org/10.1007/s00710-022-00788-w>

- Kaygusuz A, Güloğlu ZS, Aydınçakır E, Yücel C, Vural A et al. (2024). U–Pb zircon dating, Sr–Nd whole-rock and Lu–Hf zircon isotope analyses of the Eocene Arslandede pluton, Eastern Pontides, NE Turkey: implications for mantle source and magma evolution. *Geochemistry*. <https://doi.org/10.1016/j.chemer.2024.126080>
- Kelemen PB, Yogodzinski GM, Scholl DW (2003). Along-strike variation in the Aleutian island arc: genesis of high-Mg# andesite and implications for continental crust. In: Eiler J (editor) *Inside the Subduction Factory*, volume 138. Geophysical Monograph. Washington, DC, USA: American Geophysical Union, pp. 223-276. <https://doi.org/10.1029/138GM11>
- Keskin M, Pearce JA, Mitchell JG (1998). Volcano-stratigraphy and geochemistry of collision volcanism on the Erzurum–Kars plateau, northeastern Turkey. *Journal of Volcanology and Geothermal Research* 85 (1-4): 355-404. [https://doi.org/10.1016/S0377-0273\(98\)00063-8](https://doi.org/10.1016/S0377-0273(98)00063-8)
- Keskin M, 2002. FC-Modeler: a Microsoft® Excel© spreadsheet program for modeling Rayleigh fractionation vectors in closed magmatic systems. *Computers and Geosciences*. 28 (8): 919-928. [https://doi.org/10.1016/S0098-3004\(02\)00010-9](https://doi.org/10.1016/S0098-3004(02)00010-9)
- Keskin M, Pearce JA, Kempton PD, Greenwood P (2006). Magma-crust interactions and magma plumbing in a postcollisional setting: geochemical evidence from the Erzurum–Kars volcanic plateau, eastern Turkey. *Geological Society, London, Special Publications* 409: 475-505. [https://doi.org/10.1130/2006.2409\(23\)](https://doi.org/10.1130/2006.2409(23))
- Keskin M, Genç ŞC, Tüysüz O (2008). Petrology and geochemistry of post-collisional Middle Eocene volcanic units in North-Central Turkey: evidence for magma generation by slab breakoff following the closure of the Northern Neotethys Ocean. *Lithos* 104 (1-4): 267-305. <https://doi.org/10.1016/j.lithos.2007.12.011>
- Klemme S (2004). The influence of Cr on the garnet-spinel transition in the Earth's mantle: experiments in the system MgO–Cr<sub>2</sub>O<sub>3</sub>–SiO<sub>2</sub> and thermodynamic modelling. *Lithos* 77 (1-4): 639-646. <https://doi.org/10.1016/j.lithos.2004.03.017>
- Konak N, Hakyemez HY (2001). Tectonic units of the easternmost part of the Pontides: stratigraphical and structural implications. *Proceedings of the 2nd International Symposium on the Petroleum Geology and Hydrocarbon Potential of the Black Sea Area*. Turkish Association of Petroleum Geologists, Special Publication 4: 93-103.
- Konak N, Hakyemez HY (2008). 1:100 000 ölçekli Türkiye Jeoloji Haritaları No: 95. Tortum–H47 paftası. Ankara, Türkiye: Maden Tetkik ve Arama Genel Müdürlüğü Jeoloji Etütleri Dairesi.
- Le Maitre RW, Bateman P, Woolley AR, Zanettin B, Dudek A et al. (1989). *A Classification of Igneous Rocks and Glossary of Terms*. Oxford, UK: Blackwell Scientific.
- Liew TC, Hofman AW (1988). Precambrian crustal components, plutonic associations, plate environment of the Hercynian fold Belt of Central Europe: indications from a Nd and Sr isotopic study. *Contributions to Mineralogy and Petrology* 98: 129-138. <https://doi.org/10.1007/BF00402106>
- Maden N, Gelişli K, Eyüboğlu Y, Bektaş O (2009). Two-and-three-dimensional crustal thickness of the Eastern Pontides (NE Turkey). *Turkish Journal of Earth Sciences* 18 (2): 225-238. <https://doi.org/10.3906/yer-0703-3>
- Macdonald R, Hawkesworth CJ, Heath E (2000). The Lesser Antilles volcanic chain: a study in arc magmatism. *Earth Science Reviews* 49: 1-76. [https://doi.org/10.1016/S0012-8252\(99\)00069-0](https://doi.org/10.1016/S0012-8252(99)00069-0)
- McKenzie D, O'Nions RK (1991). Partial melt distributions from inversion of rare earth element concentrations. *Journal of Petrology* 32 (5): 1027-1091. <https://doi.org/10.1093/ptrology/32.5.1021>
- McCulloch MT, Gamble JA (1991). Geochemical and geodynamical constraints on subduction zone magmatism. *Earth and Planetary Science Letter* 102 (3-4): 358-374. [https://doi.org/10.1016/0012-821X\(91\)90029-H](https://doi.org/10.1016/0012-821X(91)90029-H)
- McCulloch MT, Kyser TK, Woodhead JD, Kinsley L (1994). Pb–Sr–Nd–O isotopic constraints on the origin of rhyolites from the Taupo Volcanic zone of New Zealand: evidence for assimilation followed by fractionation of basalt. *Contributions to Mineralogy and Petrology* 115: 303-312. <https://doi.org/10.1007/BF00310769>
- Morimoto M, Fabries J, Ferguson AK, Ginzburg IV, Ross M et al. (1988). Nomenclature of pyroxenes. *Mineralogical Magazine* 52 (367): 535-550. <https://doi.org/10.1180/minmag.1988.052.367.15>
- Münker C, Wörner G, Yogodzinski G, Churikova T (2004). Behaviour of high field strength elements in subduction zones: constraints from Kamchatka–Aleutian arc lava. *Earth and Planetary Science Letters* 224 (3-4): 275-293. <https://doi.org/10.1016/j.epsl.2004.05.030>
- Okay AI, Sahinturk O (1997). Geology of the eastern Pontides. In: Robinson AG (editor). *AAPG Memoir 68: Regional and Petroleum Geology of the Black Sea and Surrounding Region*. Tulsa, OK, USA: American Association of Petroleum Geologists, pp. 291-311.
- Okay AI, Leven EJ (1996). Stratigraphy and paleontology of the Upper Paleozoic sequences in the Pulur (Bayburt) region, Eastern Pontides. *Turkish Journal of Earth Sciences* 5 (2): 145-155.
- Okay AI, Tüysüz O (1999). Tethyan sutures of northern Turkey. *Geological Society Special Publications* 156: 475-515. <https://doi.org/10.1144/GSL.SP.1999.156.01.22>
- Özdamar Ş (2016). Geochemistry and geochronology of late Mesozoic volcanic rocks in the northern part of the Eastern Pontide Orogenic Belt (NE Turkey): implications for the closure of the Neo-Tethys Ocean. *Lithos* 248-251: 240-256. <https://doi.org/10.1016/j.lithos.2016.01.007>
- Özdamar Ş, Roden MF, Billor MZ (2017). Petrology of the shoshonitic Çambaşı pluton in NE Turkey and implications for the closure of the Neo-Tethys Ocean: insights from geochemistry, geochronology and Sr–Nd isotopes. *Lithos* 284-285: 477-492. <https://doi.org/10.1016/j.lithos.2017.04.025>

- Öztürk S, Kaya A (2019). A study on the characteristics of Gümüşhane seismicity: analyses of region-time parameters. *Sigma Journal of Engineering and Natural Sciences* 37 (2): 551-561.
- Pearce JA, Norry ML (1979). Petrogenetic implications of Ti, Zr, Y, and Nb variations in volcanic rocks. *Contributions to Mineralogy and Petrology* 69: 33-47. <https://doi.org/10.1007/BF00375192>
- Pearce JA (1983). The role of sub-continental lithosphere in magma genesis at destructive plate margins. Nantwich, England: Shiva, pp. 230-249.
- Pearce JA, Bender JF, De Long SE, Kidd WSF, Low PJ et al. (1990). Genesis of collision volcanism in eastern Anatolia Turkey. *Journal of Volcanology and Geothermal Research* 44 (1-2): 189-229. [https://doi.org/10.1016/0377-0273\(90\)90018-B](https://doi.org/10.1016/0377-0273(90)90018-B)
- Plank T, Langmuir CH (1998). The chemical composition of subducting sediment and its consequences for the crust and mantle. *Chemical Geology* 145 (3-4): 325-394. [https://doi.org/10.1016/S0009-2541\(97\)00150-2](https://doi.org/10.1016/S0009-2541(97)00150-2) Renne PR, Swisher CC, Deino AL, Karner DB, Owens TL et al. (1998). Intercalibration of standards, absolute ages and uncertainties in  $^{40}\text{Ar}/^{39}\text{Ar}$  dating. *Chemical Geology* 145 (1-2): 117-152. [https://doi.org/10.1016/S0009-2541\(97\)00159-9](https://doi.org/10.1016/S0009-2541(97)00159-9)
- Renne PR, Mundil R, Balco G, Min K, Ludwig KR (2010). Joint determination of  $^{40}\text{K}$  decay constants and  $^{40}\text{Ar}^*/^{40}\text{K}$  for the Fish Canyon sanidine standard, and improved accuracy for  $^{40}\text{Ar}/^{39}\text{Ar}$  geochronology. *Geochimica et Cosmochimica Acta* 74 (18): 5349-5367. <https://doi.org/10.1016/j.gca.2010.06.017>
- Renne PR, Balco G, Ludwig KR, Mundil R, Min K (2011). Response to the comment by W.H. Schwarz et al. on "Joint determination of  $^{40}\text{K}$  decay constants and  $^{40}\text{Ar}^*/^{40}\text{Ar}$  for the Fish Canyon sanidine standard, and improved accuracy for  $^{40}\text{Ar}/^{39}\text{Ar}$  geochronology" by P.R. Renne et al. 2010. *Geochimica et Cosmochimica Acta* 75 (17): 5097-5100. <https://doi.org/10.1016/j.gca.2011.06.021>
- Robertson AHF, Ustaömer T, Parlak O, Ünlügenç UC, Taşlı K et al. (2006). The Berit transect of the Tauride thrust belt, S Turkey: late Cretaceous-early Cenozoic accretionary/collisional processes related to closure of the Southern Neotethys. *Journal of Asian Earth Sciences* 27 (1): 108-145. <https://doi.org/10.1016/j.jseas.2005.02.004>
- Rollinson H (1993). *Using Geochemical Data: Evaluation, Presentation, Interpretation*. Singapore: Longman Scientific and Technical.
- Ruffet G, Féraud G, Amouric M (1991). Comparison of  $^{40}\text{Ar}/^{39}\text{Ar}$  conventional and laser dating of biotites from the North Trégor Batholith. *Geochimica et Cosmochimica Acta* 55 (6): 1675-1688. [https://doi.org/10.1016/0016-7037\(91\)90138-U](https://doi.org/10.1016/0016-7037(91)90138-U)
- Ruffet G, Féraud G, Ballèvre M, Kiénastr JR (1995). Plateau ages and excess argon in phengites: an  $^{40}\text{Ar}/^{39}\text{Ar}$  laser probe study of Alpine micas (Sesia Zone, Western Alps, northern Italy). *Chemical Geology (Isotopic Geoscience Section)* 121 (1-4): 327-343. [https://doi.org/10.1016/0009-2541\(94\)00132-R](https://doi.org/10.1016/0009-2541(94)00132-R)
- Şengör AMC, Yılmaz Y (1981). Tethyan evolution of Turkey: a plate tectonic approach. *Tectonophysics* 75 (3-4): 181-241. [https://doi.org/10.1016/0040-1951\(81\)90275-4](https://doi.org/10.1016/0040-1951(81)90275-4)
- Şen C (2007). Jurassic volcanism in the Eastern Pontides: Is it rift related or subduction related? *Turkish Journal of Earth Sciences* 16 (4): 523-539.
- Saydam Eker Ç, Arı UV (2020). Geochemistry of the Middle Jurassic sediments in Gümüşhane, north-eastern Turkey: implications for weathering and provenance. *Geological Journal* 55 (7): 4954-4976. <https://doi.org/10.1002/gj.3726>
- Shaw DM (1970). Trace element fractionation during anatexis. *Geochimica et Cosmochimica Acta* 34 (2): 237-259. [https://doi.org/10.1016/0016-7037\(70\)90009-8](https://doi.org/10.1016/0016-7037(70)90009-8)
- Smith EI, Sanchez A, Walker JD, Wang K (1999). Geochemistry of mafic magmas in the Hurricane Volcanic field, Utah: implications for small- and large-scale chemical variability of the lithospheric mantle. *The Journal of Geology* 107: 433-448. <https://doi.org/10.1086/314355>
- Staudigel H, Davies GR, Hart SR, Marchant KM, Smith BM (1995). Large scale isotopic Sr, Nd and O isotope anatomy of altered oceanic crust: DSDP/ODP sites 417/418. *Earth and Planetary Sciences* 130: 169-185.
- Stern RJ, Moghadam HS, Pirouz M, Mooney W (2021). The geodynamic evolution of Iran. *Annual Review of Earth and Planetary Sciences* 49: 9-36. <https://doi.org/10.1146/annurev-earth-071620-052109>
- Stracke A (2012). Earth's heterogeneous mantle: a product of convection-driven interaction between crust and mantle. *Chemical Geology* 330-331: 274-299. <https://doi.org/10.1016/j.chemgeo.2012.08.007>
- Sun S, McDonough WF (1989). Chemical and isotopic systematics of oceanic basalts: implications for mantle compositions and processes. In: Saunders AD, Norry MJ (editors). *Magmatism in the Ocean Basins*. Geological Society, London, Special Publications 42: 312-345. <https://doi.org/10.1144/GSL.SP.1989.042.01.19>
- Taylor SR, McLennan SM (1985). *The continental crust: its composition and evolution*. Oxford, UK: Blackwell Scientific Publication, p. 312.
- Temel A, Gündoğdu MN, Gourgand A, Le Pennec JL (1998). Ignimbrites of Cappadocia (Central Anatolia, Turkey): petrology and geochemistry. *Journal of Volcanology and Geothermal Research* 85 (1-4): 447-471. [https://doi.org/10.1016/S0377-0273\(98\)00066-3](https://doi.org/10.1016/S0377-0273(98)00066-3)
- Temizel İ, Arslan M, Ruffet G, Peucat JJ (2012). Petrochemistry, geochronology and Sr-Nd isotopic systematic of the Tertiary collisional and post-collisional volcanic rocks from the Ulubey (Ordu) area, eastern Pontide, NE Turkey: implications for extension-related origin and mantle source characteristics. *Lithos* 128-131: 126-147. <https://doi.org/10.1016/j.lithos.2011.10.006>
- Temizel İ, Arslan M, Yücel C, Abdioğlu E, Ruffet G (2016). Geochronology and geochemistry of Eocene-aged volcanic rocks around the Bafra (Samsun, N Turkey) area: constraints for the interaction of lithospheric mantle and crustal melts. *Lithos* 258-259: 92-114. <https://doi.org/10.1016/j.lithos.2016.04.023>

- Temizel İ, Arslan M, Yücel C, Abdioğlu Yazar E, Kaygusuz A et al. (2019). U-Pb geochronology, bulk-rock geochemistry and petrology of late cretaceous syenitic plutons in the Gökkyöy (Ordu) area (NE Turkey): implications for magma generation in a continental arc extension triggered by slab roll-back. *Journal of Asian Earth Science* 171: 305-320. <https://doi.org/10.1016/j.jseaes.2019.01.004>
- Temizel I, Arslan M, Yücel C, Abdioğlu Yazar E, Kaygusuz A et al. (2020). Eocene tonalite–granodiorite from the Havza (Samsun) area, northern Turkey: adakite-like melts of lithospheric mantle and crust generated in a post-collisional setting. *International Geology Review* 62: 1131-1158. <https://doi.org/10.1080/00206814.2019.1625077>
- Thirlwall MF, Smith TE, Graham AM, Theodorou N, Hollings P et al. (1994). High field strength element anomalies in arc lavas; source or process? *Journal of Petrology* 35: 819-838. <https://doi.org/10.1093/petrology/35.3.819>
- Topuz G, Altherr R, Kalt A, Satır M, Werner O et al. (2004). Aluminous granulites from the Pulur complex NE Turkey: a case of partial melting, efficient melt extraction and crystallization. *Lithos* 72 (3-4): 183-207. <https://doi.org/10.1016/j.lithos.2003.10.002>
- Topuz G, Altherr R, Siebel W, Schwarz WH, Zack T et al. (2010). Carboniferous high-potassium I-type granitoid magmatism in the Eastern Pontides: The Gümüşhane pluton (NE Turkey). *Lithos* 116 (1-2): 92-110. <https://doi.org/10.1016/j.lithos.2010.01.003>
- Topuz G, Okay AI, Altherr R, Schwarz WH, Siebel W et al. (2011). Post-collisional adakite-like magmatism in the Ağvanis massif and implications for the evolution of the Eocene magmatism in the Eastern Pontides (NE Turkey). *Lithos* 125 (1-2): 131-150. <https://doi.org/10.1016/j.lithos.2011.02.003>
- Ustaömer T, Robertson AHE, Ustaömer PA, Gerdes A, Peytcheva I (2013). Constraints on Variscan and Cimmerian magmatism and metamorphism in the Pontides (Yusufeli-Artvin area), NE Turkey from U-Pb dating and granite geochemistry. *Geological Society Special Publications* 372: 49-74. <https://doi.org/10.1144/SP372.13>
- Uysal İ, Şen AD, Ersoy EY, Dilek Y, Saka S et al. (2014). Geochemical make-up of oceanic peridotites from NW Turkey and the multi-stage melting history of the Tethyan upper mantle. *Mineralogy and Petrology* 108 (1): 49-69. <https://doi.org/10.1007/s00710-013-0277-3>
- Varol E, Temel A, Gourgaud A, Bellon H (2007). Early Miocene adakite-like volcanism in the Balkuyumcu region, central Anatolia, Turkey: petrology and geochemistry. *Journal of Asian Earth Science* 30 (5-6): 613-628. <https://doi.org/10.1016/j.jseaes.2007.02.002>
- Vervoort JD, Blichert-Toft J (1999). Evolution of the depleted mantle Hf isotope evidence from juvenile rocks through time. *Geochimica et Cosmochimica Acta* 63 (3-4): 533-556. [https://doi.org/10.1016/S0016-7037\(98\)00274-9](https://doi.org/10.1016/S0016-7037(98)00274-9)
- Vervoort JD, Plank T, Prytulak J (2011). The Hf-Nd isotopic composition of marine sediments. *Geochimica et Cosmochimica Acta* 75 (20): 5903-5926. <https://doi.org/10.1016/j.gca.2011.07.046>
- Wang XX, Wang T, Happala I, Lu XX (2002). Genesis of mafic enclaves from rapakivi-textured granites in the Qinling and its petrological significance: evidence of elements and Nd, Sr isotopes. *Acta Petrologica Sinica* 21: 935-946 (in Chinese with English abstract).
- Weaver B, Wood DA, Tarney J, Joron JL (1987). Geochemistry of ocean island basalt from the South Atlantic: Ascension, Bouvet, St. Helena, Gough and Tristan da Cunda. In: Fitton JG, Upton BGI (editors). *Alkaline Igneous Rocks*. Geological Society, London, Special Publications 30: 253-267. <https://doi.org/10.1144/GSL.SP.1987.030.01.11>
- Wilson M (1989). *Igneous Petrogenesis*. Oxford, UK: Oxford University Press.
- Winchester JA, Floyd PA (1976). Geochemical magma type discrimination: application to altered and metamorphosed basic igneous rocks. *Earth and Planetary Science Letters* 28 (3): 459-469. [https://doi.org/10.1016/0012-821X\(76\)90207-7](https://doi.org/10.1016/0012-821X(76)90207-7)
- Woodhead JD, Hergt JM, Davidson JP, Eggins SM (2001). Hafnium isotope evidence for 'conservative' element mobility during subduction zone processes. *Earth and Planetary Science Letters* 192 (3): 331-346. [https://doi.org/10.1016/S0012-821X\(01\)00453-8](https://doi.org/10.1016/S0012-821X(01)00453-8)
- Yang W, Niu H, Shan Q, Luo Y, Sun W et al. (2012). Late Paleozoic calc-alkaline to shoshonitic magmatism and its geodynamic implications, Yuximolegai area, western Tianshan, Xinjiang, Gondwana Research 22 (1): 325-340. <https://doi.org/10.1016/j.gr.2011.10.008>
- Yılmaz S, Boztug D (1996). Space and time relations of three plutonic phases in the Eastern Pontides, Turkey. *International Geology Review* 38: 935-956. <https://doi.org/10.1080/00206819709465373>
- Yılmaz Y, Tuysuz O, Yigitbas E, Genc SC, Sengör AMC (1997). Geology and tectonic evolution of the Pontides. In: Robinson AG (editor). *AAPG Memoir 68: Regional and Petroleum Geology of the Black Sea and Surrounding Region*. Tulsa, OK, USA: American Association of Petroleum Geologists, pp. 183-226.
- Yücel C, Arslan M, Temizel İ, Abdioğlu Yazar E, Ruffet G (2017). Evolution of K-rich magmas derived from a net veined lithospheric mantle in an ongoing extensional setting: geochronology and geochemistry of Eocene and Miocene volcanic rocks from Eastern Pontides (Turkey). *Gondwana Research* 45: 65-86. <https://doi.org/10.1016/j.gr.2016.12.016>
- Yücel C (2019). Geochronology, geochemistry, and petrology of adakitic Pliocene–Quaternary volcanism in the Şebinkarahisar (Giresun) area, NE Turkey. *International Geology Review* 61 (6): 754-777. <https://doi.org/10.1080/00206814.2018.1461029>
- Yücel C, Aydınçakır E, Kaygusuz A, Arslan M, Yi K et al. (2024). Petrogenesis of Late Cretaceous A-type plutonic rocks from the Eastern Pontides Orogenic Belt (NE Turkey): constraints from zircon U-Pb geochronology, zircon Lu-Hf and whole-rock Sr-Nd-Pb-Hf isotopes. *International Geology Review* 66 (11): 2055-2078. <https://doi.org/10.1080/00206814.2023.2269447>
- Zindler A, Hart SR (1986). Chemical geodynamics. *Annual Review of Earth and Planetary Sciences* 14: 493-571. <https://doi.org/10.1146/annurev.ea.14.050186.002425>

**Supplementary information**

Supplementary information is available at the following link: <https://aperta.ulakbim.gov.tr/record/273730>